Tellus SERIES B CHEMICAL AND PHYSICAL METEOROLOGY
PUBLISHED BY THE INTERNATIONAL METEOROLOGICAL INSTITUTE IN STOCKHOLM

Variability of the ocean carbon cycle in response to the North Atlantic Oscillation

By KATHRIN M. KELLER[1,2]*, FORTUNAT JOOS[1,2], CHRISTOPH C. RAIBLE[1,2], VALENTINA COCCO[1,2], THOMAS L. FRÖLICHER[3], JOHN P. DUNNE[4], MARION GEHLEN[5], LAURENT BOPP[5], JAMES C. ORR[5], JERRY TJIPUTRA[6,7], CHRISTOPH HEINZE[6,7], JOACHIM SEGSCHNEIDER[8], TILLA ROY[9] and NICOLAS METZL[9], *[1]Climate and Environmental Physics, Physics Institute, University of Bern, Sidlerstrasse 5, 3012 Bern, Switzerland; [2]Oeschger Centre for Climate Change Research, University of Bern, Zähringerstrasse 25, 3012 Bern, Switzerland; [3]Program in Atmospheric and Oceanic Sciences, Princeton University, 300 Forrestal Road, Princeton, NJ 08544-0710, USA; [4]NOAA/GFDL, 201 Forrestal Road, Princeton, NJ 08540-6649, USA; [5]Laboratoire du Climat et de l'Environnement (LSCE), L'Orme des Merisiers Bât. 712, 91191, Gif sur Yvette, France; [6]Department of Geophysics, University of Bergen, Allégaten 70, 5007 Bergen, Norway; [7]Bjerknes Centre for Climate Research, Allégaten 55, 5007, Bergen, Norway; [8]Max-Planck-Institut für Meteorologie, Bundesstrasse 53, 20146 Hamburg, Germany; [9]Laboratoire d'Océanographie et du Climat (LOCEAN/IPSL), 4 place Jussieu, 75252 Paris, CEDEX 05, France*

(Manuscript received 10 May 2012; in final form 25 October 2012)

ABSTRACT

Climate modes such as the North Atlantic Oscillation (NAO), representing internal variability of the climate system, influence the ocean carbon cycle and may mask trends in the sink of anthropogenic carbon. Here, utilising control runs of six fully coupled Earth System Models, the response of the ocean carbon cycle to the NAO is quantified. The dominating response, a seesaw pattern between the subtropical gyre and the subpolar Northern Atlantic, is instantaneous (<3 months) and dynamically consistent over all models and with observations for a range of physical and biogeochemical variables. All models show asymmetric responses to NAO^+ and NAO^- forcing, implying non-linearity in the connection between NAO and the ocean carbon cycle. However, model differences in regional expression and magnitude and conflicting results with regard to air–sea flux and CO_2 partial pressure remain. Typical NAO-driven variations are ± 10 mmol/m^3 in the surface concentration of dissolved inorganic carbon and alkalinity and ± 8 ppm in the air–sea partial pressure difference. The effect on the basin-wide air–sea CO_2 flux is small due to compensating fluxes on the sub-basin scale. Two models show a reduced carbon sink in the north-eastern North Atlantic during negative NAO phases, qualitatively in accordance with the observed decline during a phase of predominantly negative NAO. The results indicate that wind-driven dynamics are the main driver of the response to the NAO, which – via vertical mixing, upwelling and the associated entrainment of dissolved inorganic carbon and nutrients – leave an imprint on surface pCO_2 and the air–sea CO_2 flux as well as on biological export production, pH and the calcium carbonate saturation state. The biogeochemical response to the NAO is predominantly governed by vertical exchange between the surface and the thermocline; large-scale horizontal transport mechanisms are of minor importance.

Keywords: North Atlantic Oscillation, carbon cycle, ocean biogeochemistry, climate modeling, ocean-atmosphere interaction

1. Introduction

The North Atlantic Ocean, constituting the second largest natural carbon sink right after the Southern Ocean, is of eminent importance for the global carbon cycle (e.g. Sabine et al., 2004, Gerber and Joos, 2010). However, the correct

*Corresponding author.
email: keller@climate.unibe.ch

Citation: Tellus B 2012, **64**, 18738, http://dx.doi.org/10.3402/tellusb.v64i0.18738

assessment and interpretation of the North Atlantic carbon system is challenging since (1) observations are scarce and limited either in time or space and (2) the climate system in this area features significant modes of natural variability, e.g. the North Atlantic Oscillation (NAO).

Here, utilising control runs of six Earth System Models (NCAR CSM1.4 and CCSM3, GFDL ESM2.1, IPSL-CM4-LOOP, BCCR BCM-C and MPI-ESM), the natural variability of the North Atlantic carbon cycle in response to the NAO is investigated. The purpose of this study is to identify the underlying mechanisms behind the climate-carbon system in the North Atlantic which, hopefully, helps in interpreting observations, i.e. making the distinction between natural variability and anthropogenically forced climate change.

In the last 200 yr, mankind emitted large amounts of carbon dioxide through (1) combustion of fossil fuels (oil, carbon and natural gas), (2) land-use change (mainly large-scale deforestation) and (3) industrial processes such as cement production (e.g. Hegerl et al., 2007). During this period, starting with the industrialisation and sometimes referred to as 'Anthropocene' (Crutzen and Stoermer, 2000), the global carbon cycle has been brought out of steady state. Due to the continuous carbon emissions, atmospheric CO_2 has increased from about 280 ppm (preindustrial) to 391.05 ppm (September 2012), a concentration higher than ever measured in ice core records covering the past 800 000 yr (Lüthi et al., 2008). In combination with other forcing agents (e.g. CH_4 and N_2O), these CO_2 concentrations have pushed the global climate system towards conditions that have probably not occurred over the past 20 million years (Blackford and Gilbert, 2007) and at a speed unprecedented at least during the last 22 000 yr (Joos and Spahni, 2008). The atmospheric CO_2 concentrations illustrate the complex nature of the global carbon cycle – from the 257 PgC emitted to the atmosphere between 1960 and 2007 (Boden et al., 2010), only 56% remained airborne. The estimated oceanic uptake is 33%, and the remaining 11% are assumed to be taken up by the terrestrial biosphere (Sarmiento et al., 2010). Since carbon cycle and climate system are in a state of mutual dependency and steady interaction, a sound knowledge of the processes taking place is necessary to correctly detect past and present trends and, based on this, make robust projections for the future. In this context, it is essential to take into account that long-term trends and natural variability have the potential to enhance or mask each other (e.g. Latif et al., 1997; Frölicher et al., 2009; Dolman et al., 2010; McKinley et al., 2011), making it sometimes difficult to draw clear conclusions.

The NAO is a large-scale climate phenomenon and the dominating mode of weather and climate variability in the Northern Atlantic. Constituting a seesaw in atmospheric mass between a subtropical high-pressure system and a subpolar low-pressure system (Bjerknes, 1964), NAO involves large changes in air surface temperature, wind, storminess and precipitation. In the ocean, NAO implies changes in heat content, gyre circulations, mixed-layer depth, salinity, high latitude deep water formation and sea-ice cover (Hurrell and Deser, 2009). A positive NAO phase (i.e. an increased pressure gradient between the two systems) is linked to positive sea-surface temperature (SST) anomalies in the subtropics, negative anomalies in the subpolar gyre (Cayan, 1992; Cullen et al., 2001) and the corresponding winter mixing: due to changes in ocean convection, regions with warmer SSTs experience less vigorous winter mixing than normal and vice versa (Dickson et al., 1996). Mechanisms and the current state of knowledge with respect to the NAO are given in review articles (e.g. Wanner et al., 2001, Pinto and Raible, 2012 and references therein).

A number of modelling studies have addressed the connection between NAO and North Atlantic Ocean carbon cycle utilising global ocean general circulation models (McKinley et al., 2004; Thomas et al., 2008; Ullman et al., 2009; Levine et al., 2011; Tjiputra et al., 2012), coupled ecosystem-circulation models of the North Atlantic (Friedrich et al., 2006; Löptien and Eden, 2010) and a single atmosphere-ocean general circulation model (AOGCM) (Patara et al., 2011). In accordance with observations (e.g. Bates et al., 2002), these modelling studies identified variations in wind-induced mixing and SST as the driving mechanisms of the response of ocean biogeochemistry. In the subpolar gyre, the carbon cycle in the upper ocean is mainly governed by mixing-driven entrainment of dissolved inorganic carbon (DIC) from nutrient-enriched deeper layers to the surface; air–sea gas exchange is of minor importance. In the subtropics, changes in SST are the dominating factor. Matter of debate are the importance of the biological pump (e.g. McKinley et al., 2004, Löptien and Eden, 2010) and advective transport processes during periods of persistent negative or positive NAO forcing (e.g. Thomas et al., 2008).

In the next section, the six models are described and evaluated. In the result section, first the response of ocean physics and biogeochemistry to the NAO is presented. Then, the results are compared with observations. In the discussion section, the results are summarised and compared with observations and earlier model studies. Finally, conclusions are given.

2. Models and evaluation

2.1. Models

This study is based on simulations performed with six fully coupled 3-D atmosphere-ocean climate models, each of

them including additional carbon cycle modules covering the terrestrial and oceanic biosphere. An overview is given in Table 1.

2.1.1. NCAR CCSM3-BEC. The Community Climate System Model Version 3 (CCSM3), based on the framework of the Community Climate System Model (CCSM) project (Blackmon et al., 2001), was developed by the National Center for Atmospheric Research (NCAR) in Boulder, USA. The 'standard' model includes components for atmosphere, ocean, sea ice and land surface, all linked by a coupler exchanging fluxes and state information between the components (Collins et al., 2006a). The atmospheric component, Community Atmosphere Model version 3 (CAM3; Collins et al., 2006b), has a horizontal resolution of approximately 3.75° and 26 vertical levels. The land component, Community Land Surface Model version 3 (CLM3; Oleson et al., 2004), possesses the same horizontal grid as the atmosphere. The ocean component is represented by the Parallel Ocean Program (POP) ocean general circulation model (Smith and Gent, 2004) and integrated on a dipole grid. The horizontal resolution is on average 3.6° in longitude and 0.8° to 1.8° in latitude, and the vertical dimension features 25 unevenly distributed levels (5 levels for the top 100 m, 13 for the top 1000 m) extending to a depth of 4750 m. The sea-ice component, Community Sea Ice Model version 5.0 (CSIM5; Briegleb et al., 2004), features the same horizontal grid as the ocean model. Ocean biogeochemistry is represented by the Biogeochemical Elemental Cycling Model (BEC), consisting of modules for the upper ocean ecology (Moore et al., 2004) and full-depth biogeochemistry (Doney et al., 2006). The marine ecosystem component is based on traditional phytoplankton-zooplankton-detritus-nutrient food web models (e.g. Fasham et al., 2001) and includes (1) the nutrients nitrate, ammonium, phosphate, dissolved iron and silicate, (2) four groups of phytoplankton, (3) zooplankton, (4) dissolved organic matter (DOM) and (5) sinking particulate detritus. $CaCO_3$ production is included in phytoplankton. The biogeochemical module comprises the cycling of carbon, oxygen, nitrogen, phosphorus, silicon and iron.

2.1.2. NCAR CSM1.4-carbon. The CSM1.4-carbon climate model (Fung et al., 2005; Doney et al., 2006) was developed by the NCAR in Boulder, USA. The fundament of the model is a modified version of the NCAR CSM1.4 coupled physical model, consisting of ocean, atmosphere, land and sea-ice components linked by a flux coupler (Boville et al., 2001). The atmospheric component CCM3 has a horizontal resolution of 3.75° and 18 vertical levels (Kiehl et al., 1998). The ocean component is the NCAR CSM Ocean Model (NCOM) with 25 levels in the vertical and a resolution of 3.6° in longitude and 0.8° to 1.8° in latitude (Gent et al., 1998). Similar to the CCSM3, the components for sea ice and ocean as well as land surface and atmosphere run on the same horizontal resolution. The CSM1.4-carbon model comprises a modified version of the terrestrial biogeochemistry model CASA (Carnegie-Ames-Stanford Approach; Randerson et al., 1997) and a prognostic version of the OCMIP ocean biogeochemistry model (Najjar et al., 2007). The ocean biogeochemical model includes the main processes of the organic and inorganic carbon cycle within the ocean and air–sea CO_2 flux. The biological productivity within the ocean model is controlled by temperature, solar irradiance, mixed-layer depth, phosphate and iron.

Table 1. Major model characteristics

Model	Model ID	Atmosphere	Land carbon	Ocean	Ocean carbon	References
NCAR CCSM3-BEC	CCSM3	CAM3 3.75° × 3.75°, 26	CLM3	POP (0.8 − 1.8°) × 3.6°, 25	BEC	Moore et al., 2004 Doney et al., 2006
NCAR CSM1.4-carbon	CSM1.4	CCM3 3.75° × 3.75°, 18	CASA	NCOM (0.8 − 1.8°) × 3.6°, 25	prognostic OCMIP	Najjar et al., 2007
GFDL ESM2.1	GFDL	AM2.1 2° × 2.5°, 24	LM3	MOM-4 1/3° to 1°, 50	TOPAZ	Dunne et al., 2005 Dunne et al., 2007
MPI-ESM	MPIM	ECHAM6 1.9° × 1.9°, 31	JSBACH	MPIOM 1.5° × 1.5°, 40	HAMOCC5.1	Maier-Reimer et al., 2005
BCCR BCM-C	BCCR	ARPEGE 2.8° × 2.8°, 31	LPJ	MICOM 0.8° to 2.4°, 34	HAMOCC5.1	Maier-Reimer et al., 2005 Assmann et al., 2010
IPSL-CM4-LOOP	IPSL	LMDZ-4 3° × 3°, 19	ORCHIDEE	OPA-8 2° × 2°, 31	PISCES	Aumont et al., 2003

2.1.3. GFDL ESM2.1. The ESM2.1 earth system model was developed by the Geophysical Fluid Dynamics Laboratory (GFDL) in Princeton, USA, the physical fundament of the model being the CM2.1 coupled climate model (Delworth et al., 2006). In a fully coupled state, the model includes components for ocean (MOM-4; Griffies et al., 2004), atmosphere (AM2.1) and terrestrial biosphere (LM3; Anderson et al., 2004). AM2.1 has a horizontal resolution of 2.5° longitude by approximately 2° latitude and a vertical resolution of 24 levels. LM3 is based on potential vegetation, so no land use is included. MOM-4 has 50 vertical levels (22 10-m levels in the upper 220 m), its spatial resolution is nominally 1° globally, with a higher resolution of 1/3° near the equator. Ocean biogeochemistry is represented by TOPAZ (Dunne et al., 2005; Dunne et al., 2007) and includes a number of major nutrients (N, P, Si and Fe), both labile and semi-labile dissolved organic pools and parameterisations to represent the microbial loop (Henson et al., 2010). The ocean ecosystem is based on three classes of phytoplankton, and biological productivity is modelled as a function of chl:C ratios and limited by nutrients and light. Also a simplified version of the ocean iron cycle is included, comprising biological uptake and remineralisation, particle sinking and scavenging and adsorption/desorption.

2.1.4. MPI-ESM. The Earth System Model run at the Max-Planck-Institute for Meteorology (MPIM) in Hamburg, Germany, consists of the atmospheric model ECHAM6 with embedded Jena Scheme for Biosphere–Atmosphere coupling in Hamburg (JSBACH) terrestrial biosphere model and the MPIOM physical ocean model, which further includes a sea-ice model (Marsland et al., 2003). Biogeochemistry is represented by the Hamburg Ocean Carbon Cycle (HAMOCC) 5.1 marine biogeochemistry model (Maier-Reimer et al., 2005), which is implemented into the MPIOM ocean model and integrated on a coordinate system with a nominal resolution of 1.5°. The North Pole is located over Greenland, allowing a good coverage of the Nordic Seas. The vertical resolution is 40 levels, with higher resolution in the upper part of the water column (10 m at the surface to 13 m at 90 m). The coupling between the different components is done by using the OASIS coupler (Terray et al., 1995). The concept behind HAMOCC5.1 is to address large-scale and long-term features of the marine carbon cycle, and it is not designed to give a complete description of the marine ecosystem. Marine biological productivity is temperature dependent following Eppley (1972) and is limited by the availability of phosphorous, nitrate, iron and light. The export production is split between opal and calcite producers depending on the availability of silicate.

2.1.5. BCCR BCM-C. The Bergen Earth system model (BCM-C; Tjiputra et al., 2010) was developed at the Bjerknes Centre for Climate Research (BCCR) in Bergen, Norway. The atmosphere is represented by the spectral atmospheric general circulation model ARPEGE from Météo France (Furevik et al., 2003) with a horizontal resolution of about $2.8° \times 2.8°$. A total of 31 vertical levels is employed, ranging from the surface to 0.01 hPa (20 layers in the troposphere). The ocean component is an updated version of the Miami Isopycnic Coordinate Ocean Model (MICOM; Bleck et al., 1992), featuring horizontal grid spacing of approximately $2.4° \times 2.4°$ and 34 isopycnic vertical layers. For a better resolution of the dynamics near the equator, the horizontal spacing in the meridional direction is gradually decreased to 0.8° along the equator. The sea-ice model is the original model integrated into the MICOM ocean model, consisting of one ice and one snow layer assuming a linear temperature profile in each layer. All the components are, similar to MPIM, linked using the OASIS coupler. The ocean biogeochemistry component is the same as in the MPIM model, HAMOCC5.1 (Maier-Reimer et al., 2005), but adopted to and re-tuned for use on isopycnal coordinates and the flow field of the MICOM dynamical model (Assmann et al., 2010). The terrestrial biogeochemistry is represented by the Lund-Postdam-Jena Model (LPJ; Sitch et al., 2003), a large-scale terrestrial carbon cycle model with a horizontal resolution of approximately $2.5° \times 2.5°$. It implements dynamical vegetation (including terrestrial photosynthesis, respiration, resource competition, tissue turnover, dynamic vegetation population with 10 plant functional types (PFTs), soil organic and litter dynamic as well as natural fire occurrence) but does not take land-use change into account.

2.1.6. IPSL-CM4-LOOP. The IPSL-CM4-LOOP model was developed at the Institut Pierre-Simon Laplace (IPSL), Paris, France. Its component units are the Laboratoire de Météorologie Dynamique atmospheric model (LMDZ-4) with a horizontal resolution of approximately $3° \times 3°$ and 19 vertical levels (Hourdin et al., 2006), coupled to the OPA-8 ocean model with a horizontal resolution of $2° \times 2°$ and 31 vertical levels and the LIM sea-ice model (Madec et al., 1998). The land biosphere is represented by the global vegetation model ORCHIDEE (Krinner et al., 2005) and the marine carbon cycle by the PISCES model (Aumont et al., 2003). PISCES includes the cycling of carbon, oxygen and the major nutrients, two phytoplankton size classes (nanophytoplankton and diatoms) and two zooplankton size classes (microzooplankton and mesozooplankton). Phytoplankton growth is limited by the availability of nutrients, temperature and light.

2.2. Model evaluation

Since the focus of the study is on the intrinsic variability of the climate-carbon system, the analysis is based on control runs; that is, CO_2 emissions are set to zero and other forcings are set to constant preindustrial levels. A prerequisite when working with control runs is the assumption that the models are in quasi-steady state. Since the spin-up time is not necessarily an appropriate measure to verify this assumption, we evaluated the drift of the model runs for each grid cell by linear regression. In our area of interest, the North Atlantic (10° to 80°N and 80°W to 20°E), the models show maximal surface trends in DIC (mmol/m^3/decade) and SST (°C/decade) of 0.04/0.00 (CCSM3), 0.05/0.00 (CSM1.4), 0.04/0.00 (GFDL), 0.56/0.02 (BCCR), 0.00/0.00 (MPIM) and 0.00/0.00 (IPSL). The comparably high values for BCCR originate from a few grid cells at the northern boundary of the region while the drift is much smaller in most of the North Atlantic. Overall the drift is negligible. For a subset of the models, an evaluation of historical simulations can be found in Schneider et al. (2008) and Roy et al. (2011). Figure. 1 shows the annual mean differences between control simulations and observations of the variables DIC, alkalinity and PO_4. In this context the absence of forcing in the model data has to be accounted for. This holds in particular for the concentrations of DIC, which have been increasing over the anthropocene due to the uptake of anthropogenic CO_2. Also to be considered has the fact that the observational data is likely not representing real annual averages. Both points confine a simple one-to-one comparison. Compared to observations of DIC and alkalinity (Key et al., 2004), four models match the observed pattern with only small deviations. Two models (BCCR and IPSL) tend to overestimate the surface concentrations of these two variables in large parts of the North Atlantic. For PO_4 (Garcia et al., 2010), four out of six models show too low concentrations in the northern North Atlantic. Towards the south, five out of six models overestimate PO_4. One reason for this discrepancy between the models is the implementation of the iron cycle. In CSM1.4 and MPIM, the positive offset of PO_4 is caused by a too strong iron limitation of biological production (Schneider et al., 2008; Steinacher et al., 2010). However, all models reasonably capture the observed large-scale patterns of the concentrations.

To investigate the interannual variability, the standard deviation along the annual means was calculated (not shown). For all models and all three variables the highest variability can be found in the subpolar gyre and the adjacent northern regions. However, the magnitude of these large-scale variations differs significantly between the models. The standard deviations of DIC (mmol/m^3), Alk (mmol/m^3) and PO_4 (mmol/m^3) reach values of up to 20/25/0.06 (CCSM3), 25/30/0.09 (CSM1.4), 6/10/0.05 (GFDL), 10/15/0.02 (BCCR), 20/25/0.05 (MPIM) and 20/25/0.12 (IPSL). For the two NCAR models, the annual means of the control runs were compared with historical simulations (years 1980–2009). The spatial patterns of all three variables are similar in both simulations. The same holds true for the concentration of PO_4 in the CCSM3, and the CSM1.4 however shows lower historical PO_4 levels in the subpolar gyre (up to -0.1 mmol/m^3). Surface DIC is higher in both historical simulations, up to 60 mmol/m^3 in the subtropical and 35 mmol/m^3 in the subpolar gyre. Historical surface Alk concentrations are slightly higher (up to 25 mmol/m^3) in the subtropics. In the subpolar gyre, the models are not in accordance (CCSM3: $+10$ mmol/m^3; CSM1.4: up to -35 mmol/m^3).

The NAO is defined by an empirical orthogonal function (EOF) analysis of sea level pressure (SLP) in the North Atlantic area (30° to 80°N and 100°W to 40°E). Prior to the EOF analysis, the SLP field is area-weighted to account for the convergence of meridians on a latitude–longitude grid (Baldwin et al., 2009). The leading EOF patterns of the six models (Fig. 2c) capture reasonably well the spatial structure of the NAO, yet the explained variability varies significantly. The NAO is known to be most pronounced during winter. The observation-based leading EOFs of winter (DJF), spring (MAM), summer (JJA) and autumn (SON) explain 39.44, 32.92, 27.21 and 23.17% (www.cgd.ucar.edu/cas/jhurrell/indices.info.html, access: 08.05.2012). The models yield explained variances of 52.3, 47.7, 40.9 and 38.1% (CCSM3), 42.5, 39.1, 42.7 and 32.6% (CSM1.4), 37.6, 37.7, 36.7 and 32.5% (GFDL), 36.6, 30.1, 40.2 and 31.3% (BCCR), 35.9, 31.8, 31.3 and 33.4% (MPIM) and 37.7, 37.6, 31.4 and 39.4% (IPSL), missing the seasonal variability of the NAO signal. The observation-based NAO index shows some low-frequency variability, e.g. a period of mainly negative NAO from approximately 1960–1980 followed by a NAO$^+$ phase during the 1990s. Compared to this, the NAO time series of the six models (Fig. 2a) are relatively unstable. The autocorrelation of the winter NAO time series (Fig. 2b) indicates some decadal-scale variability which is not captured by the models. This lack of variability, a known and prevalent issue in climate modelling (Parker et al., 2007), is possibly due to the usage of control runs; based on a multi-model study, Osborn (2004) suggests that the observed variability of the NAO is not only intrinsic, but at least partly driven by external greenhouse gas forcing. However, for the most part the autocorrelation of the observations is within the model range.

Based on the two NCAR models, the required time period of model data was evaluated. In each case 200 yr of monthly data were investigated, and the results proved to be stable for time periods of approximately $\geq$60 yr

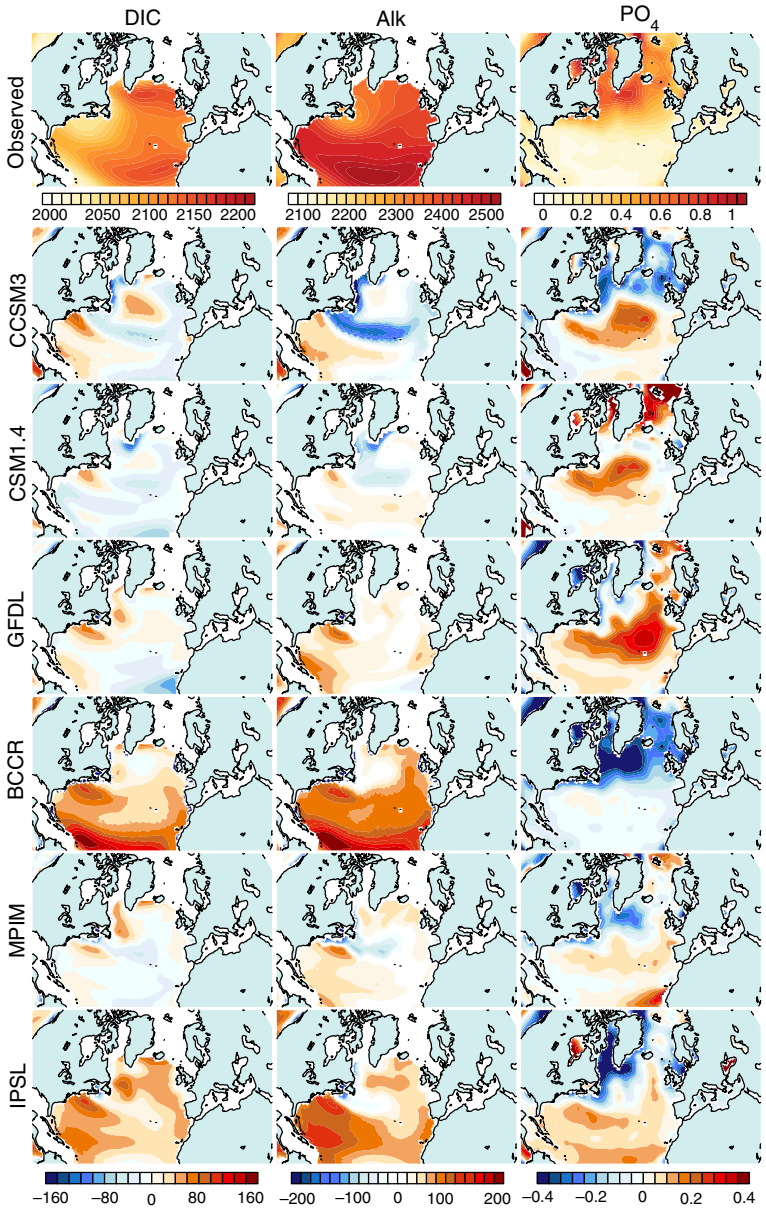

Fig. 1. Top row: Observed annual climatology of dissolved inorganic carbon (DIC; mmol/m^3), alkalinity (Alk; mmol/m^3) – both taken from Key et al. (2004), and PO_4 (mmol/m^3) – taken from Garcia et al. (2010). Below: The difference between the simulated concentrations and the observations. DIC and Alk, originally μmol/kg, were converted using the annual salinity and SST fields of Garcia et al. (2010).

(CCSM3) and $\geq$45 yr (CSM1.4). So, for good measure as well as computational reasons, it was decided to perform the analysis on 100 yr of monthly data. Furthermore, it was decided to focus on the winter (DJF) season since (1) the NAO is known to be most pronounced during winter and (2) tests based on annual data resulted in the expected closely related, yet weaker response of the ocean. Despite the different explained variances of the EOF patterns, the results support the assumption that the findings of this study are valid and not the consequence of a misrepresentation, i.e. over- or underestimation of the NAO. A number of analysis techniques were applied, including cross correlation, linear regression and composite analysis. Since the results showed consistency, it was decided to restrict the presented results to correlation and composite analysis. In a similar spirit, the following presentation strategy is adopted to make it easier for the reader to follow the arguments and to limit the number of figures to a reasonable

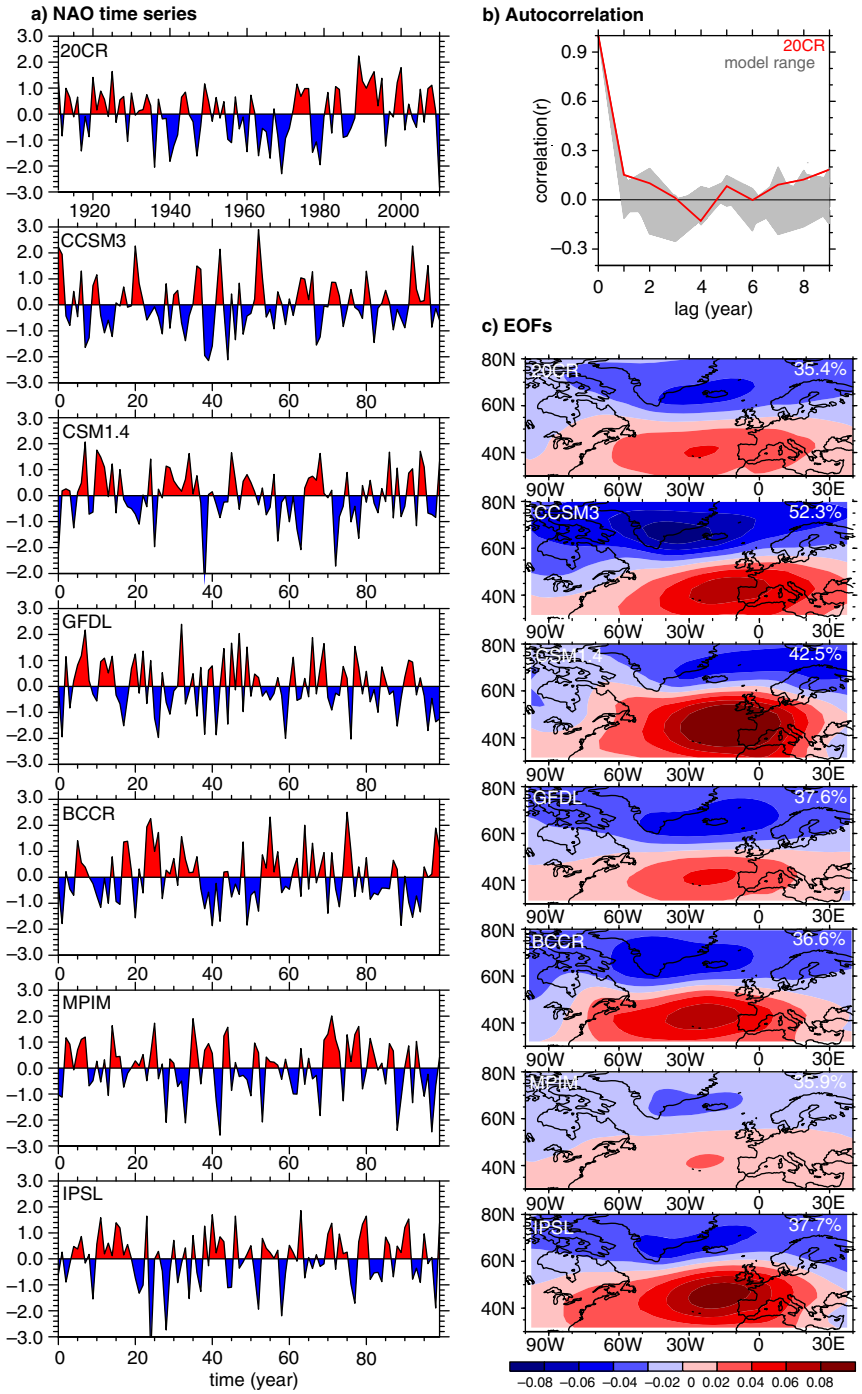

Fig. 2. a) Standardised winter (DJF) NAO indices for the 20CR dataset (years 1911–2010; Compo et al. 2011) and all six models. b) Autocorrelation r of the winter NAO index for 20CR (red) and the model range (grey). c) The corresponding EOF 1 patterns of winter sea level pressure in the North Atlantic region (30: 80°N, 100°W: 40°E).

amount. First, our findings are discussed using results of a single model and a broad set of variables. Then, the range of models is compared for a more restricted set of key variables to illustrate robustness of findings and variations among the models. We note that the more complete analysis was carried out for all models. The CCSM3 simulation is used to introduce results since it was performed by the group of the first authors (Steinacher et al., 2010) and relatively easy access to also less common output is possible.

3. Results

3.1. Ocean physics

Figure. 3 shows the response of ocean physics to the NAO based on the CCSM3 model. Both correlations and composites represent the winter season, and the composites are calculated for the NAO exceeding one standard deviation ($NAO > |\sigma|$). NAO^+ induces an increase (decrease) in surface wind stress in the subpolar (subtropical) Atlantic, resulting in corresponding variations of (1) mixed-layer depth (MLD) and (2) upwelling. The latter also leaves an imprint on the Atlantic Meridional Overturning Circulation (AMOC; not shown) and is the result of the emergence of a large-scale circulation (barotropic stream function, BSF) anomaly resembling the 'intergyre' gyre introduced by Bjerknes (1964) and Marshall et al. (2001). This anticyclonic (clockwise) anomaly, covering a good part of the subtropical and subpolar Atlantic, is framed by cyclonic anomalies in the north and the south.

SST is basically the inverse of wind stress and MLD, indicating large-scale stratification in the (especially western) subtropics. Surface salinity (SSS) features large-scale positive anomalies in the subpolar region. Since this pattern is closely related to MLD, DIC and PO_4 (see next section), it is presumably caused by entrainment of water masses from deeper layers to the surface. The composite patterns for NAO^+ and NAO^- states are approximately reversed. However, differences concerning spatial patterns as well as signal-strength indicate non-linearity in the response of ocean physics to the NAO. Overall the results agree with the available observations as summarised in Hurrell and Deser (2009).

Figure. 4 presents the composite patterns ($NAO > |\sigma|$) for the winter season of MLD and upwelling for the six models. Generally speaking, all models are consistent in showing a similar physical response as discussed for the CCSM3, in particular when recalling the differences in explained SLP variance by the NAO for the different models. MLD and SST (not shown) clearly illustrate the seesaw pattern between the subpolar and subtropical regions while BSF (not shown) and the corresponding upwelling exhibit the imprint on the gyre circulation. However, the models differ concerning strength and spatial pattern of the signal. Striking is the discrepancy between the mean states of NAO^+ and NAO^-, which is evident when the absolute anomalies are compared. With regard to MLD, the strongest response can be found locally in the subpolar Atlantic (CCSM3: 400m/ -280 m for NAO^+/NAO^-; CSM1.4: 160 m/ -175m; GFDL: 500 m/ -700 m; BCCR: 160 m/ -80 m; MPIM: 280 m/ -400 m; and IPSL: 250 m/ -300 m), the main centres of action around southern Greenland (GFDL, MPIM) or in the west (BCCR)/east (CCSM3, CSM1.4, IPSL) of it. The inverse anomalies in the subtropics are less prominent, not exceeding -40 m/60 m for NAO^+/NAO^- (MPIM). Variations of SST (not shown) range between ± 1°C in the subtropical (CCSM3, CSM1.4, MPIM) and, more localised, between -2°C for NAO^+ (CCSM3) and $+1.4$ °C for NAO^- (CSM1.4) in the subpolar gyre. In addition to this, all models show localised anomalies (up to 1.75°C (CCSM3)/ -1.2°C (BCCR) for NAO^+/NAO^-) in both the North and Norwegian Sea.

A further distinction between the models comes from the intra-annual variability of the response to NAO forcing. An investigation of the four seasons (DJF, MAM, JJA SON) illustrates that ocean dynamics (i.e. MLD and upwelling) show a response throughout the year, yet most pronounced during winter and spring. With regard to thermodynamics (e.g. SST) the models are not in accordance. The majority shows a more or less constant response throughout the year while single models show the strongest anomalies in winter/spring (BCCR) and spring/summer (CSM1.4). A comparison with the strength of the respective winter NAO signal shows that the model with the largest explained variance, the CCSM3 (52.3% explained by EOF1), has not necessarily the strongest response to NAO forcing. Despite this significant overestimation of the NAO (observation-based EOF1: 39.44%), the response of ocean physics is comparable in strength as well as significance with the models GFDL (37.6%) and BCCR (36.6%). In conclusion, a generally consistent response to winter NAO is found for ocean physics across the range of models.

3.2. Ocean biogeochemistry

Figure. 5 shows the response of ocean biogeochemistry to NAO forcing based on the CCSM3. As for ocean physics, the result is a seesaw between subtropical and subpolar gyre. Of particular prominence is the similarity between DIC and the nutrient PO_4, both featuring patterns closely related to MLD. This consensus identifies on-site entrainment as the main driver behind these anomalies rather than large-scale horizontal transport and, in case of DIC, indicates the minor importance of air–sea CO_2 exchange. This is supported by an investigation of the column inventories of DIC and PO_4 (not shown). In response to NAO^+ forcing, both variables show significant positive (negative) surface anomalies in the subpolar (subtropical) gyre. The positive anomalies in the subpolar ocean are barely visible in the column inventory, which again points towards the dominance of vertical relocation processes within the water column rather than horizontal transport or, in case of DIC, gas exchange. In contrast to this,

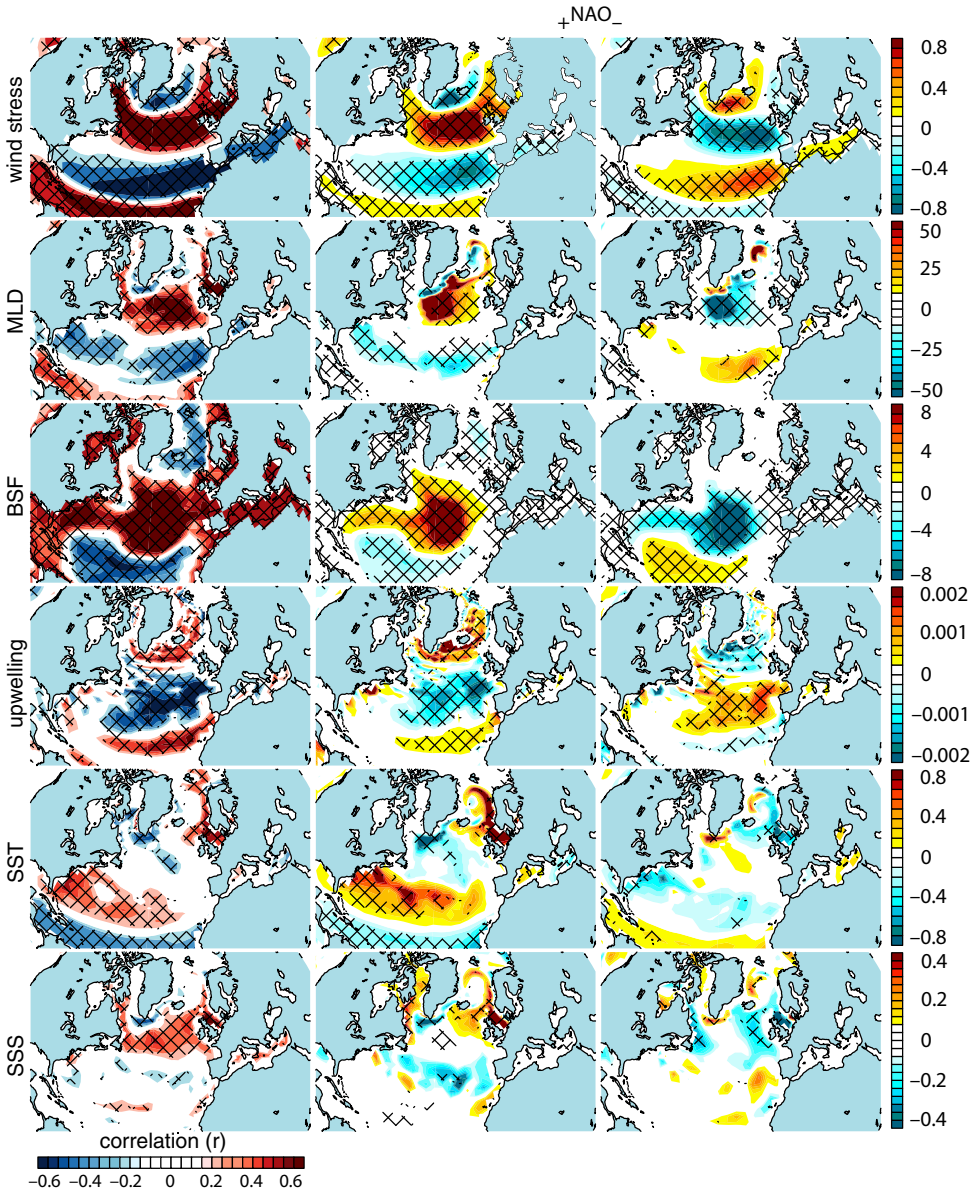

Fig. 3. CCSM3: Correlation r with NAO index (left) and composite mean patterns for prominent NAO (NAO $> |\sigma|$; right) of wind stress (dyne/cm^2), mixed-layer depth (MLD; m), barotropic stream function (BSF; Sv), upwelling (mm/s), sea-surface temperature (SST;°C) and surface salinity (SSS; g/kg). Calculations were done for the winter season and on surface level (upwelling: 75 m depth), the composites are given as anomalies and checked areas indicate statistical significance (t test, 5% level).

significant negative anomalies of both inventories can be found in the (mainly eastern) subtropics. This can be attributed to downwelling processes in that area, diluting the concentrations of DIC and PO_4 by the pumping of low-nutrient surface waters to deeper ocean layers. Further evidence is supplied by Hovmöller diagrams (not shown) of meridional transects crossing the North Atlantic which show that the increased concentrations of DIC and PO_4 in the subpolar surface ocean are indeed accompanied by negative anomalies in the subjacent ocean layers. Besides, there is no clear indication of either latitudinal or meridional horizontal transport.

The altered surface DIC and PO_4 concentrations go hand in hand with corresponding variations of (1) export production (POC; transport of particulate organic carbon out of the euphotic zone, in this case at a depth of 75 m) and (2) pCO_2 and, consequently, pH and OmegaA (the saturation state of calcite provided similar results: spatial patterns and correlation coefficients are exactly the same, the composite anomalies slightly higher – varying

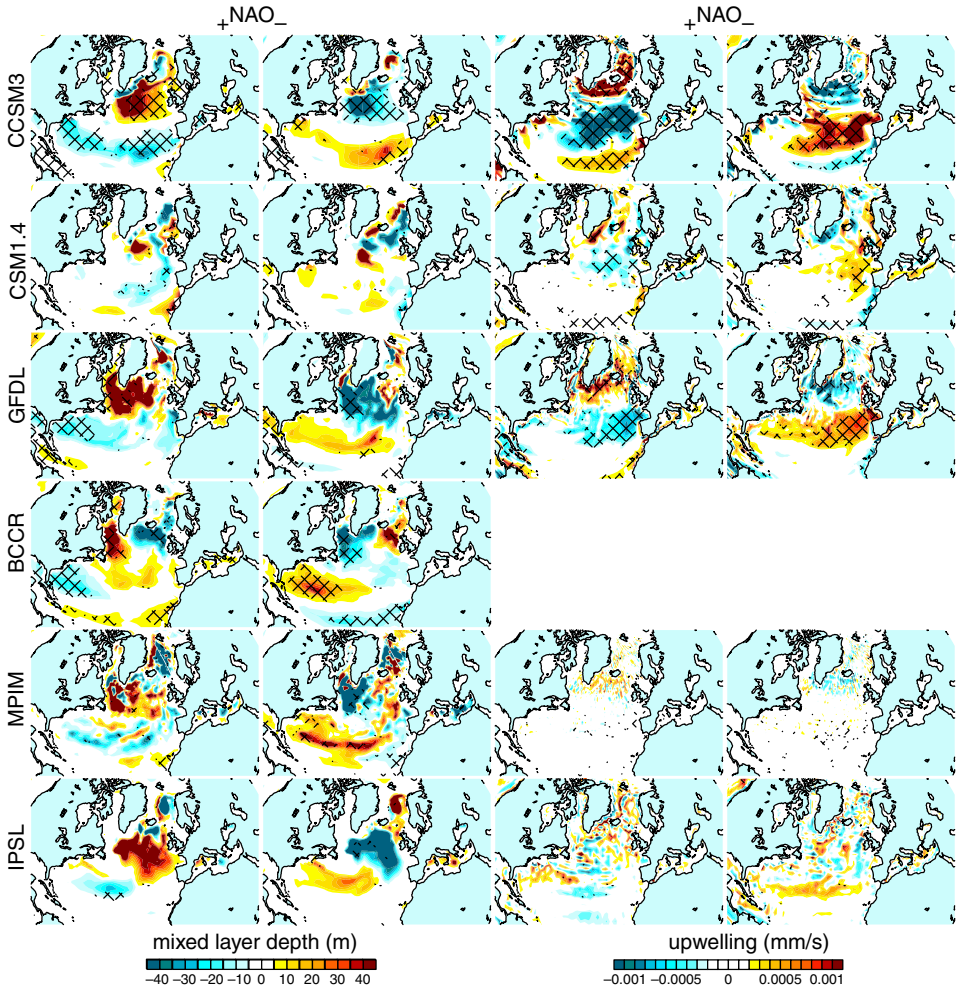

Fig. 4. Model comparison: Composite mean winter patterns for prominent NAO (NAO $> |\sigma|$) of mixed-layer depth (MLD; m) and upwelling (mm/s). Upwelling is calculated at a depth of 75 m, the composites are given as anomalies and checked areas indicate statistical significance (*t* test, 5% level). For BCCR, an isopycnic model, upwelling is not available.

between ± 0.1 for OmegaA and ± 0.16 for OmegaC). Point (1) is interesting in the sense that, although the patterns are calculated for the winter season, POC shows a significant response even in the subpolar gyre – the increased supply of nutrients results in an increase of biological production. Compared to this, calculations on an annual basis (not shown) provide a partly different response: while the increased supply of nutrients in the subpolar gyre is still accompanied by a rise in production, the decrease of nutrients in the subtropics goes hand in hand with a rise in production as well. A possible explanation for this increase in biological production, despite the reduced nutrient concentrations, could be the warming of the surface ocean due to prominent stratification. Regarding point (2), the large-scale differences between DIC and pCO_2 in the subtropics can be mainly attributed to variations in SST.

Figure. 6 presents the composite patterns (NAO $> |\sigma|$) of the variables DIC and PO_4. Overall, the response of ocean biogeochemistry is consistent across all models. Typical NAO-driven variations are ± 10 mmol/m^3 in the surface concentration of DIC, and the response of Alk is of comparable magnitude. Surface DIC shows the strongest reaction in the subpolar North Atlantic (CCSM3: $24/-28$ mmol/m^3 for NAO^+/NAO^-; CSM1.4: $16/-24$; GFDL: $5/-5$; BCCR: $3/-3$; MPIM: $12/-6$ and IPSL: $12/-12$), and the less prominent anomalies in the subtropics stay within -15 (CCSM3, CSM1.4) and 12 (IPSL) for NAO^+/NAO^-. In addition to this, a positive response to NAO forcing can be found in the Nordic Seas (all models except BCCR) and the Labrador Sea (all models except IPSL). For GFDL, BCCR and MPIM the latter can be explained with the deepening of the MLD (Fig. 4), which is supported by the corresponding positive anomalies of PO_4.

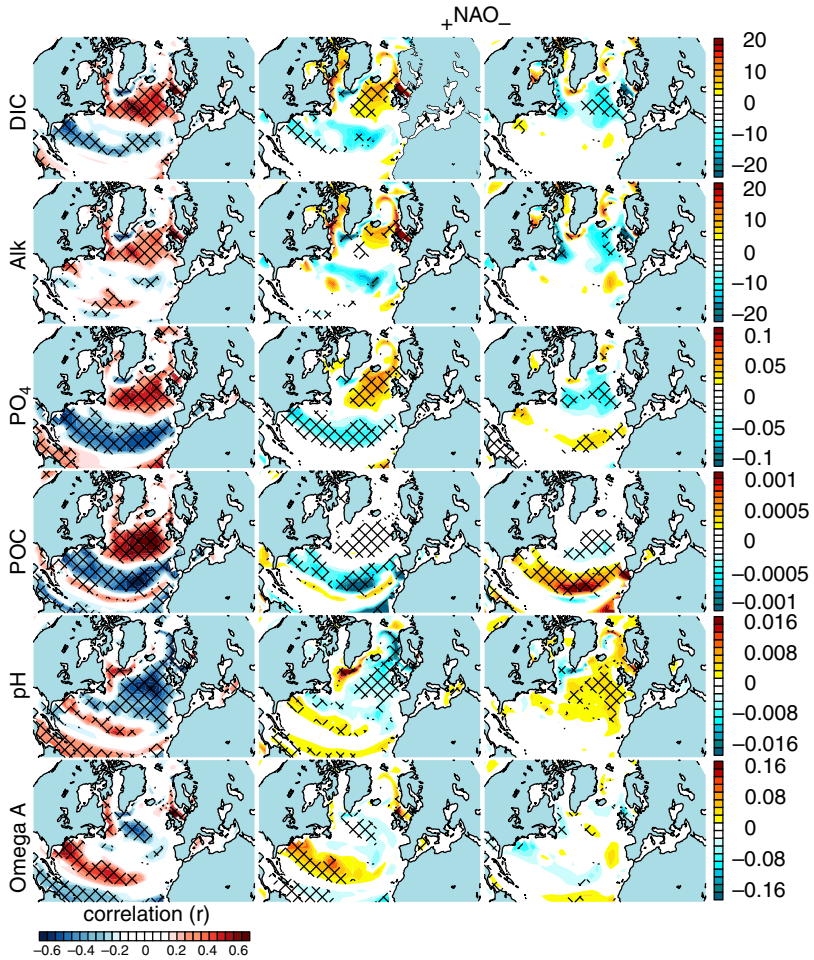

Fig. 5. CCSM3: Correlation r with NAO index (left) and composite mean patterns for prominent NAO (NAO $> |\sigma|$; right) of dissolved inorganic carbon (DIC; mmol/m^3), alkalinity (Alk; meq/m^3), PO_4 (mmol/m^3), export production (POC; mmol POC/m^3 cm/sec), total pH (Lueker et al., 2000) and the saturation state of aragonite (OmegaA). Calculations were done for the winter season and on surface level (POC: 75 m depth), the composites are given as anomalies and checked areas indicate statistical significance (t test, 5% level).

The composites of the two NCAR models indicate no connection between NAO and MLD in this area, yet it can be found in the correlation patterns (CCSM3: see Fig. 3). The positive anomaly in the Nordic Seas is likely caused by the inadequate or even missing representation of freshwater fluxes within the models. A salinity normalisation of DIC to a reference salinity of 35 psu (not shown) conserves the main feature, i.e. the seesaw pattern between subtropical and subpolar gyre. Yet, the localised anomaly in the Nordics Sea turns from positive to negative in all six models. Since the overall effect on DIC turned out to be small and the insight associated with the procedure is debated (e.g. Robbins, 2001, Friis et al., 2003), it was decided to focus on the actual concentrations.

Again the models differ concerning strength and spatial patterns of the response to the NAO. This is illustrated by the DIC composites of two NCAR models, CCSM3 and CSM1.4. The CCSM3 composite for NAO$^+$ shows significant positive (negative) anomalies in large parts of the subpolar gyre (the western subtropics). The NAO$^-$ composite roughly provides the reversed picture. Yet, the significant anomalies in the subpolar gyre are shifted in a south-eastern direction towards the European continent and the anomalies in the western subtropics feature hardly statistical significance. In contrast to this, the CSM1.4 shows no statistical significance in the subpolar gyre at all. However, significant negative (positive) anomalies can be found in the eastern (western) subtropics for NAO$^+$ (NAO$^-$). Another difference between the models concerns the seasonal cycle. As expected the majority of the models show the best correlations between NAO and surface biogeochemistry during winter and spring, with two

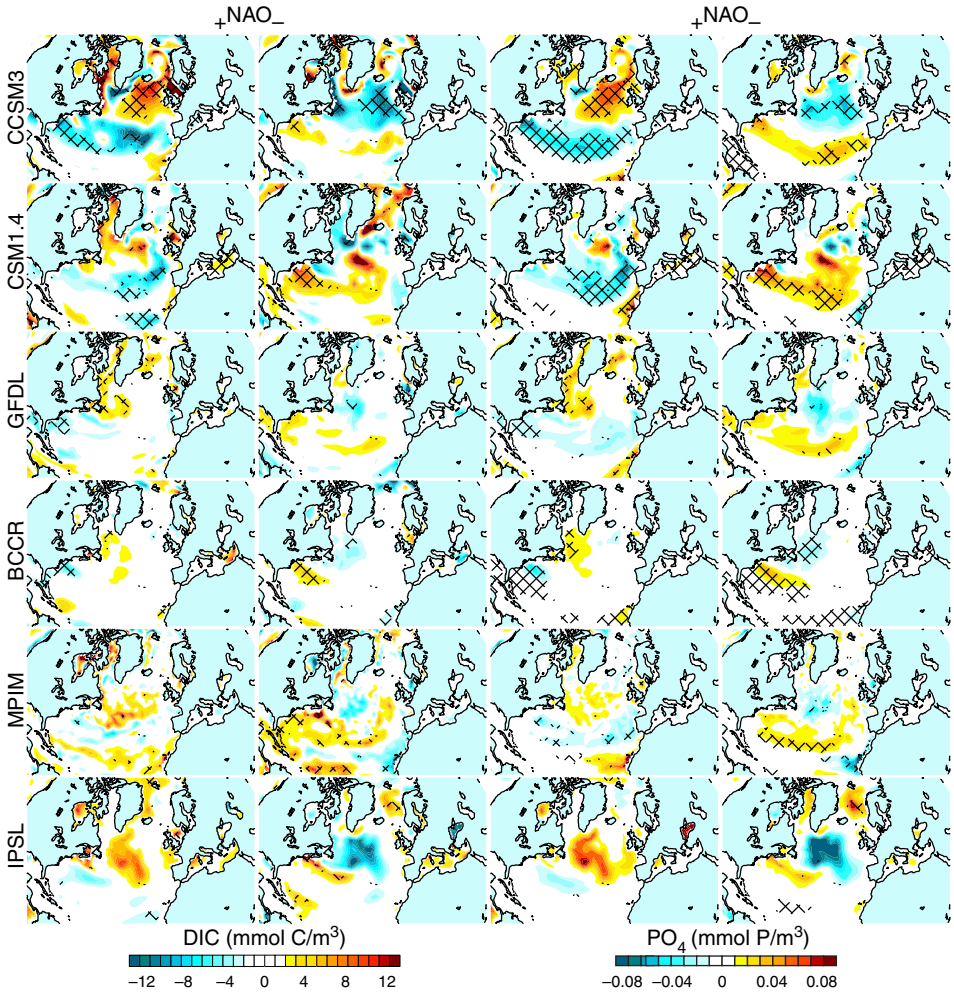

Fig. 6. Model comparison: Composite mean winter patterns for prominent NAO (NAO > |σ|) of dissolved inorganic carbon (DIC; mmol/m^3) and PO_4 (mmol/m^3). Calculations were done on surface level, the composites are given as anomalies and checked areas indicate statistical significance (*t* test, 5% level).

exceptions: the MPIM model shows correlations of comparable strength throughout the year, and IPSL features the highest values during summer and autumn. When taking the strength of the respective winter NAO signal into account it appears that, concerning DIC and PO_4, the two models with the largest explained variability (CCSM3: 52.3%; CSM1.4: 42.5%) display the strongest, statistically significant response. As for ocean physics, this is not the case for ΔpCO_2 and the CO_2 flux, supporting the assumption that the results are valid and not the consequence of a misrepresentation, i.e. overestimation of the NAO.

Next, we turn to the links between winter NAO and surface ocean pCO_2 (pCO_2^o), the gradient in pCO_2 between surface ocean and atmosphere (ΔpCO_2) and air–sea CO_2 flux. pCO_2^o is not conserved during transport, but rather a function of DIC, Alk, temperature and salinity. Changes in these variables exert often opposite influences on pCO_2^o, interfering the attribution of pCO_2^o changes to mechanisms and drivers. For instance, upwelling usually increases both DIC and Alk. However, while a rise in DIC increases pCO_2^o, a positive change in Alk shows the opposing effect, and consequently the overall change in pCO_2^o can be either positive or negative. Changes in ΔpCO_2 are further influenced by variations in atmospheric pCO_2 (pCO_2^a) due to atmospheric transport and air–sea fluxes, and the exceptions are the BCCR and GFDL models where pCO_2^a is prescribed. However, we note that the response of ΔpCO_2 to the NAO is very similar to that of pCO_2^o in all models. The air–sea carbon flux does not only vary with pCO_2^o and ΔpCO_2, but also due to changes in the primarily turbulence-dominated gas transfer velocity (e.g. Wanninkhof, 1992), parameterised as a function of wind speed in the models. Given all these complexities, we expect that the links between NAO and pCO_2^o and related

variables are not as clear and more heterogeneous across the model range as for example the links found for DIC or PO_4.

Usually the pCO_2 gradient between the surface ocean and atmosphere ($\Delta pCO_2 = pCO_2^o - pCO_2^o$) is the main driver of the air–sea CO_2 flux, and a rise in pCO_2^o and ΔpCO_2 results in a decrease of the air–sea CO_2 flux and vice versa. This is indeed the case in the western subtropical gyre, where NAO^+-induced changes of MLD and SST trigger large-scale stratification (see the CCSM3-composites in Fig. 7). This state, suppressing the entrainment of water from deeper, nutrient-enriched ocean layers, results in negative anomalies of DIC and pCO_2^o and, in turn, an increase of the air–sea CO_2 flux. The same, yet with changed signs, is found for large areas in the northern North Atlantic. In contrast, there are also some regions where the anomalies of ΔpCO_2 and air–sea CO_2 flux point in the same direction. Thus, the change in flux is not dominated by a change in the pCO_2 gradient, but by the change in the gas transfer velocity. An example can be found off Norway where, during NAO^+, significant positive anomalies of ΔpCO_2 and air–sea CO_2 flux match with increases in wind and MLD.

Figure. 7 presents the composite patterns ($NAO > |\sigma|$) of the variables ΔpCO_2 and air–sea CO_2 flux. Here, it has to be mentioned that, due to the usage of control runs, pCO_2 and ΔpCO_2 go largely hand in hand. The models BCCR and GFDL are even run with constant atmospheric CO_2 concentrations, resulting in ΔpCO_2 being simply oceanic pCO_2 minus atmospheric pCO_2 (BCCR: 287.4 ppm; GFDL: 286 ppm). As for the CCSM3 model, the air–sea CO_2 flux is mainly driven by ΔpCO_2 which, in turn, largely follows DIC. This system of dependencies is valid for all models; differences between the three variables are caused by the additional effects of wind stress (CO_2 flux) and SST, salinity, alkalinity and the formation of calcite (pCO_2). Similar to DIC, ΔpCO_2 features the strongest anomalies in the subpolar North Atlantic (CCSM3: $16/-12$ ppm for NAO^+/NAO^-; CSM1.4: $10/-8$; GFDL: $6/-5$; BCCR: $6/-6$; MPIM: $2/-4$ and IPSL: $8/-8$). The response in the subtropics ranges within ± 6 ppm for all models. Yet it is not possible to identify a distinct seesaw pattern as for DIC and PO_4, the direction of the anomalies varies on a small scale. In addition, there are large differences between the models. The same holds true for the corresponding air–sea flux of CO_2. For instance, during NAO^+ conditions increased carbon uptake occurs in the western subtropics (CCSM3, GFDL), south of Greenland (CCSM3, CSM1.4, MPIM) and the Labrador Sea (BCCR, MPIM) while a decrease in uptake is found in the eastern subpolar gyre (CCSM3, GFDL, BCCR, IPSL) and the eastern (CCSM3, CSM1.4), western (MPIM) or entire subtropics (BCCR). For the six models, the air–sea exchange of carbon is largest off Norway (CCSM3: $0.005/-0.002$ mmol/m^3 cm/s for NAO^+/NAO^-), south of Iceland (CSM1.4: $0.005/-0.007$), south and southeast of Greenland (GFDL: $-0.002/0.003$; IPSL: $0.003/-0.003$) and in the Labrador Sea (BCCR: $0.004/-0.004$; MPIM: $0.003/-0.004$). An integration of the air–sea CO_2 flux over the North Atlantic (10: 80°N; −80: 20°E) and the entire winter season (90 d) results in flux anomalies of CCSM3: $-0.0068/0.0078$ PgC for NAO^+/NAO^-, CSM1.4: $-0.0055/0.0025$, GFDL: $-2.54 \times 10^{-5}/0.0028$, BCCR: $-0.0050/0.0057$, MPIM: $-0.0015/0.0053$ and IPSL: $-0.0028/0.0050$. In relation to the winter mean state, these anomalies account for up to 5%. Globally, the integrated anomalies range between -0.024 (CCSM3) and 0.037 PgC (MPIM) for NAO^+ and between -0.014 (MPIM) and 0.051 PgC (IPSL) for NAO^-.

The importance of vertical entrainment of carbon for variations in surface DIC and air-to-sea carbon fluxes is underlined by the model CSM1.4. Due to the comparably simple formulation of the ocean biogeochemistry module, changes in DIC due to marine productivity and the remineralisation of organic matter and calcite (ΔDIC_{bio}) are linearly linked to variations in phosphate (ΔPO_4) and alkalinity (ΔAlk) according to the Redfield ratios (Redfield et al., 1963). This linear relationship allows to assign changes in DIC to (1) variations in the marine biological cycle and (2) air–sea gas exchange driven by CO_2 concentrations only (see Plattner et al., 2001, Gruber and Sarmiento, 2002, Frölicher and Joos, 2010):

$$\Delta DIC_{bio} = 117\ \Delta PO_4 + 0.5\ (\Delta Alk + 16\Delta PO_4) \quad (1)$$

$$\Delta DIC_{gas} = \Delta DIC_{total} - \Delta DIC_{bio} \quad (2)$$

In eq. (1), the terms on the right-hand side represent reorganisation processes of (1) the organic matter cycle linked to the carbon-phosphate Redfield ratio and (2) the calcite cycle. The difference between ΔDIC_{total} and ΔDIC_{bio} [eq. (2)] can be assigned to gas exchange. An investigation of the DIC composite patterns shows that DIC_{total} (Fig. 6) and DIC_{bio} (not shown) virtually feature the same pattern, DIC_{bio} with slightly higher positive as well as negative anomalies in the subpolar gyre (NAO^+: DIC_{total} varies between ± 14 mmol/m^3, DIC_{bio} between ± 17 mmol/m^3). This small discrepancy can be explained by DIC_{gas} (NAO^+: variations between ± 5 mmol/m^3) which shows positive and, on a very local scale, negative anomalies. Beyond the subpolar gyre DIC_{gas} features negative anomalies in the very eastern subtropics; however, a large part of the North Atlantic shows no response at all. In conclusion, this points out the dominance of biological processes over air–sea gas exchange. Since the former are limited by the supply of nutrients, this again indicates the importance of ocean dynamics.

3.3. *Time scale of response*

To investigate the interannual component of the ocean response to the NAO, Fig. 8 shows the anomalies of wind stress, BSF, MLD, SST and DIC of five consecutive winters dominated by NAO^+ for the model CCSM3. The increase of surface wind stress instantaneously results in corresponding anomalies of gyre circulation and MLD. An exception can be found at year 4 in the subpolar gyre where, in spite of negative anomalies of wind stress, MLD is deeper than usual. Since the pattern of this anomaly is equal to that of year 3 and the scale of magnitude is significantly smaller (year 3: up to 900 m; year 4: less than 300 m), it is presumably a remainder from the very strong anomaly in the previous year. The five SST patterns are consistent in showing the expected positive (negative) anomalies in the subtropical (subpolar) gyre. In addition, all years feature positive SST anomalies in the high north. Likewise, DIC is persistent in constituting a seesaw between negative anomalies in the subtropical and positive in the subpolar gyre and the northern North Atlantic. Neither ocean dynamics nor biogeochemistry indicate any significant large-scale horizontal transport.

Figure 9 compares time series of winter NAO with anomalies of DIC and MLD for the model CCSM3, and DIC and MLD are averaged over areas representing the subpolar (40° to 60°N, 50° to 20°W) and subtropical gyre (29° to 34°N, 67° to 61°W). All three variables vary simultaneously, confirming that the NAO-induced response of ocean dynamics and, in turn, ocean biogeochemistry is

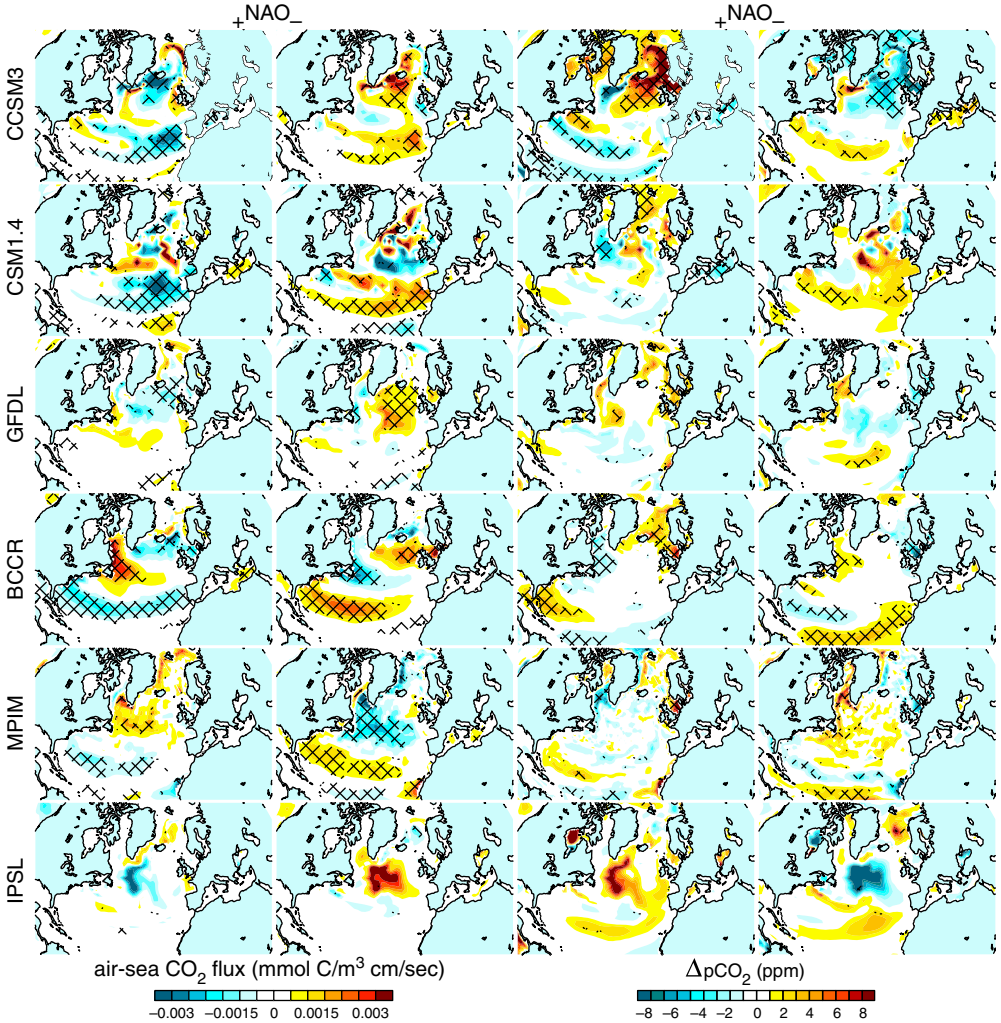

Fig. 7. Model comparison: Composite mean winter patterns for prominent NAO (NAO $> |\sigma|$) of the gradient of pCO_2 between atmosphere and ocean (ΔpCO_2) and air–sea CO_2 flux (mmol/m^3 cm/s). Calculations were done on surface level, the composites are given as anomalies and checked areas indicate statistical significance (*t* test, 5% level). The unit of ΔpCO_2 is ppmv (CCSM3, CSM1.4, MPIM) and µatm (GFDL, BCCR, IPSL), respectively. For the integrated annual air–sea CO_2 flux (mol m^{-2} yr^{-1}), multiply by 315.36.

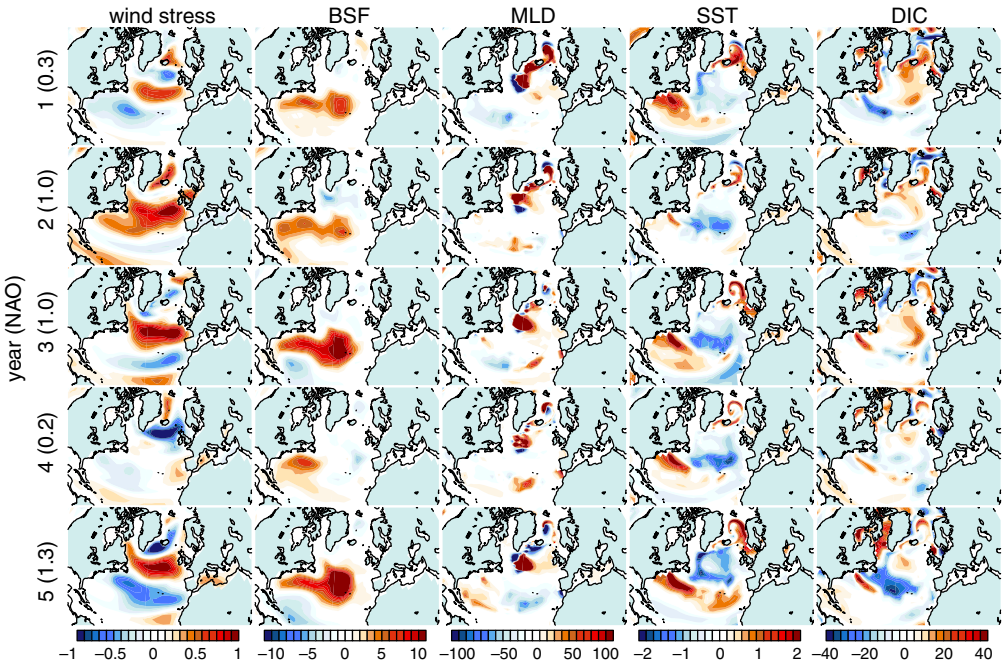

Fig. 8. CCSM3: Anomalies of wind stress (dyne/cm^2), barotropic stream function (BSF; Sv), mixed-layer depth (MLD; m), sea-surface temperature (SST; °C) and dissolved inorganic carbon (DIC; mmol/m^3) during five consecutive winter seasons with positive NAO.

instantaneous (<3 months). The two locations differ with regard to the direction of the response. In the subpolar gyre both variables are significantly correlated with the NAO (correlation r: 0.70 and 0.25 for MLD and DIC, respectively). In the subtropics MLD/DIC and NAO are anticorrelated (r: -0.34 and -0.38 for MLD and DIC, respectively), reflecting the inverse wind stress anomaly compared to the subpolar gyre. The anomalies of MLD are smaller in the subtropical than in the subpolar gyre, ranging between $-35/40$ m and $-70/125$ m, respectively. The range of DIC anomalies, however, shows hardly any difference, with values between $-19/15$ mmol/m^3 (subpolar gyre) and $-16/14$ mmol/m^3 (subtropics). Regarding the instantaneous response of the ocean to NAO forcing, further support is provided by time series on a monthly basis (not shown) which underline especially the close relationship between NAO and MLD. In this context it can be stated that the anomalies of MLD in the subpolar gyre are largest during winter and spring irrespective of the strength of the NAO. Something alike is not detectable in the subtropics and in neither case for DIC. A shift of the time series of MLD and DIC in relation to the NAO shows that (1) significant correlations can be found with lags up to 4 yr, yet (2) the highest correlation in each case is present at lag 0. This can be illustrated on the basis of DIC, with lagged correlations of 0.25 (lag 0), 0.07 (lag 1), -0.08 (lag 2), -0.21 (lag 3), -0.15 (lag 4) and 0.03 (lag 5) in the subpolar and correlations of -0.38, -0.28, 0.08, 0.32, 0.26 and -0.03 in the subtropical gyre. Striking is the high anticorrelation (relative to lag 0) at lag 3. However, this signal is put into perspective when the autocorrelation of the NAO index is taken into account (lag 1: 0.16; lag 2: -0.21; lag 3: -0.25; lag 4: -0.12; lag 5: 0.15). As can be seen, the lagged signal is not necessarily a physical response. In this case, it is likely caused by the temporal variability of the NAO.

3.4. *Models vs. observations*

A comparison with observational data is rather challenging since carbon measurements are limited in either time or space. Long-term time series are available only at a few locations while the data originating from measurement cruises is providing only a temporarily fragmented snapshot. We utilise four different datasets. The Bermuda Atlantic Time Series (BATS; e.g. Bates, 2007) is located in the western subtropics (32°50′ N, 64°10′ W) and provides monthly resolved observations since 1988. Here, we use measurements from the surface ocean (depth ≤ 8 m). The data was taken from http://bats.bios.edu/index.html, access: 20.01.2012. The subpolar gyre is represented by three datasets. One originates from the SURveillance de l'ATLANTique programme (SURATLANT; e.g. Corbière et al., 2007; Metzl et al., 2010), measured on cruises crossing the subpolar gyre between Iceland and Newfoundland. The data has a temporal resolution of roughly 3 months and was collected from 1993 to 1997 and 2001

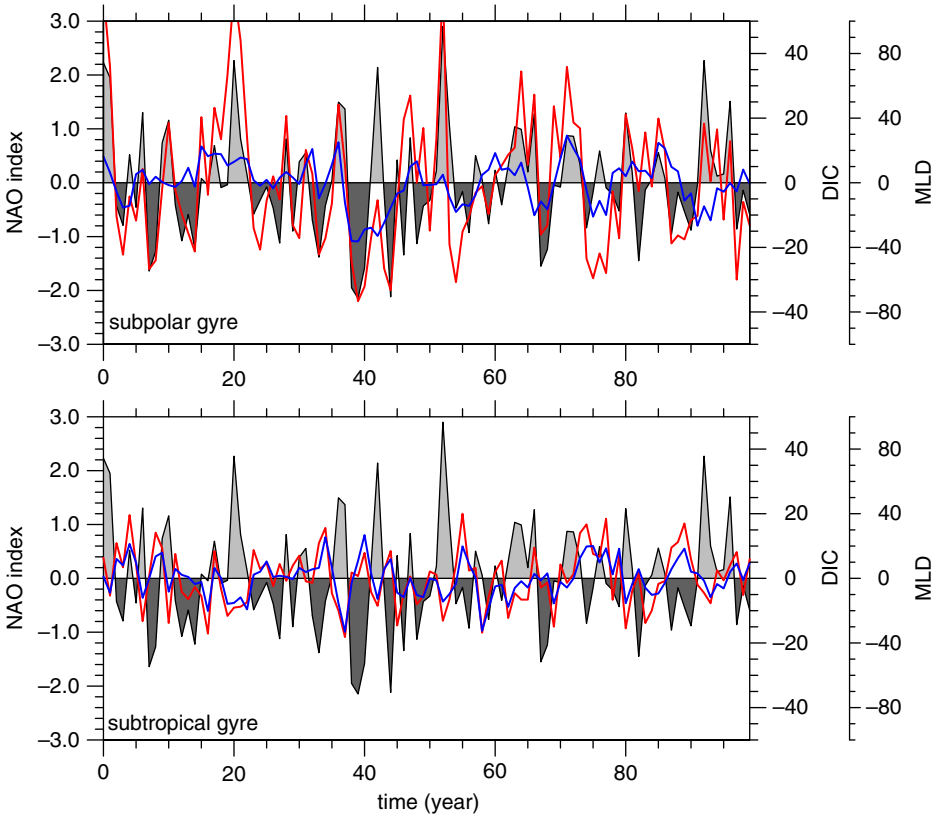

Fig. 9. CCSM3: Time series of winter NAO index (shaded), surface dissolved inorganic carbon (DIC; mmol/m^3) (blue) and mixed-layer depth (MLD; m) (red). DIC and MLD are averaged over areas in the subpolar (40: 60°N, −50: −20°E) and subtropical (29: 34°N, −67: −61°E) gyres and given as anomalies. The NAO index is standardised, arising from an EOF analysis of sea level pressure in the North Atlantic (30: 80°N, −100: 40°E).

to 2008. We utilise surface data from 50: 60°N and 40: 20°W. The other two datasets are the Irminger and Iceland Sea time series (Olafsson, 2007a, b), and both were downloaded from the CARINA database (Key et al., 2010), access: 13.04.2012. The data was collected from 62: 65°N and 15: 10° W (Iceland Sea) and 62: 65°N and 30: 20°W (Irminger Sea), the measurements started in 1983 and the sampling is seasonal. In both cases, we use surface data covering the time period 1985–2006. The observational NAO is presented by the monthly NAO time series of the NOAA Climate Prediction Center (CPC; http://www.cpc.noaa.gov/data/teledoc/telecontents.shtml, access: 19.01.2012).

Tables 2 and 3 show the correlation *r* between NAO and the variables DIC, PO_4 and SST for the four datasets and all six models. Due to the sparse and irregular sampling of the observations, we refrained from doing a statistical test. The model data is averaged over areas representing the subpolar (50: 60°N, 40: 20°W) and the subtropical gyre (29: 34°N, 67: 61°W). The variables are correlated on two temporal scales, monthly and for the winter season. For the latter, the observations comprise the available monthly values for January, February and December while the models are represented by seasonal (DJF) means. All datasets and five out of six models show higher correlations in winter than throughout the year, underlining the fact that the NAO is dominating the winter climate in the North Atlantic region. The exception is the IPSL model which, as discussed before, shows the highest seasonal correlations between NAO and surface biogeochemistry during summer and autumn.

In the western subtropics at BATS, both DIC and PO_4 are anticorrelated with the NAO, a finding consistent with all models. The only exception is IPSL which tends against zero in both cases. In contrast to the observations, the correlations for NAO/PO_4 exceed NAO/DIC for all models, with values ranging from −0.21 (GFDL) up to −0.55 (BCCR). The positive correlation of NAO/SST supports this finding, showing that the NAO-induced reduction of wind stress results in surface stratification and, consequently, less vertical nutrient supply. This is supported by the high correlation between DIC and PO_4 both in the dataset and especially in the models, putting into perspective the importance of air–sea gas exchange for

Table 2. Correlation r between monthly and seasonal (DJF) time series of NAO index and the surface variables dissolved inorganic carbon (DIC; μmol/kg), PO_4 (μmol/kg) and SST (°C) for four observational datasets

	r monthly	# monthly	r DJF	# DJF
SUBTROPICS				
BATS				
NAO/DIC	−0.08	255	−0.32	61
NAO/PO_4	−0.04	224	−0.12	55
NAO/SST	−0.04	253	0.09	60
DIC/PO_4	−0.02	224	0.02	55
DIC/SST	−0.65	253	−0.60	60
SUBPOLAR GYRE				
SURATLANT				
NAO/DIC	0.11	40	0.42	11
NAO/PO_4	0.14	30	0.24	7
NAO/SST	−0.13	40	−0.65	11
DIC/PO_4	0.83	30	0.62	7
DIC/SST	−0.84	40	−0.33	11
Iceland Sea				
NAO/DIC	0.10	77	0.26	20
NAO/PO_4	0.08	76	0.21	20
NAO/SST	0.03	77	−0.16	20
DIC/PO_4	0.90	76	0.60	20
DIC/SST	−0.82	77	−0.27	20
Irminger Sea				
NAO/DIC	0.12	81	0.15	17
NAO/PO_4	0.21	77	0.37	16
NAO/SST	−0.12	81	−0.22	17
DIC/PO_4	0.91	77	0.48	16
DIC/SST	−0.79	81	−0.55	17

One dataset is an extract from BATS (Bates, 2007), located in the western subtropics (32°50′N, 64°10′W). The subpolar gyre is represented by SURATLANT (Metzl et al., 2010), covering parts of the subpolar gyre (50 : 60°N, 40 : 20°W), and measurements done on cruises in the Irminger Sea (62 : 65°N, 30 : 20°W) and Iceland Sea (62 : 65°N, 15 : 10°W) (Olafsson, 2007a, b). The NAO is represented by the NOAA CPC monthly NAO time series (http://www.cpc.noaa.gov/data/teledoc/telecontents.shtml). The variables are correlated on two temporal scales, monthly and for the winter season. For the latter, the observations comprise the available monthly values for January, February and December.

the ocean DIC inventory. However, as for NAO/PO_4, the link between NAO/SST seems to be overestimated by the models.

In the subpolar gyre, the comparison with observational data is complicated by the small number of observations, especially for the winter season. For instance, in the SURATLANT dataset PO_4 is represented by only seven values, six of them obtained during a negative phase of the NAO. Nonetheless, observations and models are consistent in showing positive correlations for NAO/DIC and NAO/PO_4 and negative ones for NAO/SST. The only exception is the Iceland Sea dataset where, on a monthly scale, the correlation for NAO/SST is slightly positive. Taking the scarce number of observations into account, the correlations between NAO/DIC and NAO/PO_4 are of comparable strength. The models reasonably capture (CCSM3, CSM1.4, GFDL, BCCR) or tend to underestimate (MPIM, IPSL) this link. Again DIC and PO_4 are highly correlated. The negative correlation for NAO/SST is evidence for the influence of the NAO on ocean dynamics, in this case reduced vertical mixing.

The direct impact of the NAO on the ocean carbon cycle was further evaluated conducting linear regressions between NAO index and surface DIC concentrations. Here, the regression slopes correspond to a change of one standard deviation σ in the NAO index. In the subtropics at BATS, a one σ increase is linked to a decrease in surface DIC of -2 mmol/m^3 (monthly) and -5 mmol/m^3 (DJF), respectively. On the monthly scale, the models capture (CCSM3, CSM1.4) or slightly underestimate the observation-based values. For winter the models are consistent in underestimating the response to the NAO, with values ranging from -1 mmol/m^3 (GFDL, MPIM and IPSL) to -3 mmol/m^3 (CCSM3, CSM1.4).

For the subpolar gyre, the SURATLANT dataset provides values of 2.5/5 mmol/m^3 (monthly/DJF). The Irminger

Table 3. Correlation r between monthly and seasonal (DJF) time series of NAO index and the surface variables dissolved inorganic carbon (DIC; mmol/m^3), PO_4 (mmol/m^3) and SST (°C) for the six models

		SUBTROPICS		SUBPOLAR GYRE	
Model	Variables	r monthly	r DJF	r monthly	r DJF
CCSM3	NAO/DIC	−0.11	−0.38	0.09	0.48
	NAO/SST	0.06	0.35	−0.04	−0.20
	DIC/PO_4	0.82	0.84	0.96	0.99
CSM1.4	NAO/DIC	−0.03	−0.27	0.05	0.25
	NAO/SST	0.03	0.35	−0.05	−0.03
	DIC/PO_4	0.75	0.80	0.94	0.91
GFDL	NAO/DIC	−0.05	−0.11	0.04	0.40
	NAO/SST	0.03	0.23	−0.04	−0.23
	DIC/PO_4	0.75	0.82	0.99	0.93
BCCR	NAO/DIC	−0.01	−0.26	0.05	0.23
	NAO/SST	0.03	0.42	−0.06	−0.42
	DIC/PO_4	0.78	0.71	0.97	0.78
MPIM	NAO/DIC	−0.02	−0.19	0.08	0.12
	NAO/SST	0.03	0.29	−0.06	−0.11
	DIC/PO_4	0.66	0.72	0.97	0.93
IPSL	NAO/DIC	−0.06	0.01	0.21	0.08
	NAO/SST	−0.13	0.03	−0.18	−0.08
	DIC/PO_4	0.55	0.50	1.0	0.99

The model data is averaged over areas representing the subpolar (50: 60°N, −40: −20°E) and the subtropical gyre (29: 34°N, 67: 61°W), the NAO is defined by an EOF analysis of sea level pressure in the North Atlantic (30: 80°N, 100°W: 40°E). The variables are correlated on two temporal scales, monthly and for the winter season. For the latter, the models are represented by seasonal (DJF) means.

and Iceland Sea time series both feature values of approximately 3/3 mmol/m^3 (monthly/DJF). The models show the same tendency as SURATLANT, with larger values during winter. Yet there are differences. The two NCAR models feature values of 4/6 mmol/m^3 (monthly/DJF), exceeding the observations on both time scales. GFDL, MPIM and IPSL show anomalies of 2/4 mmol/m^3 (monthly/DJF), the weakest response can be found for the BCCR model with 0/2 mmol/m^3 (monthly/DJF).

4. Discussion

The variability of the ocean carbon cycle in response to the NAO has been analysed utilising six Earth System Models. The results are consistent over all models, yet relative and absolute magnitudes differ among models and regions. The response of the North Atlantic carbon cycle, a seesaw pattern between the subtropical gyre and the subpolar Northern Atlantic, was found to be instantaneous (<3 months). The results indicate wind-driven dynamics as the main driver of the response, which – via vertical mixing, upwelling and the associated entrainment of DIC – leave an imprint on surface pCO_2 and, consequently, the air–sea CO_2 flux. While there is ample evidence that the NAO impacts large-scale ocean circulation (e.g. Curry and McCartney, 2001; Raible et al., 2001; Marshall et al., 2001; Flatau et al., 2003; Jakobsen et al., 2003; Visbeck et al., 2003), till now there has been no definite answer if this connection has a significant influence on the ocean carbon cycle. We find no lead in this direction, even when analysing consecutive years with persistent NAO. Our results suggest that it is of relatively minor importance compared to wind-driven mixing processes.

The results proved to be stable, independent of investigated time period (DJF versus annual values) or analysis technique (correlation, regression versus composite patterns). For a NAO^+ phase, the results indicate the following chain of events (summarised in Fig. 10). First, the increase in wind causes a positive anomaly in gyre circulation which covers a substantial part of the subtropical and subpolar Atlantic. This anticyclonic anomaly, resembling the 'intergyre' gyre introduced by Bjerknes (1964) and Marshall et al. (2001), is framed by negative, cyclonic anomalies in the North and South. In the entire North Atlantic, the gyre circulation is accompanied by the corresponding upwelling. Second, the increased surface wind stress in some (more northern) areas leads to a deepening of MLD and, following this and partly in accordance with increased upwelling, entrainment of DIC, Alk and PO_4. The higher nutrient supply to the euphotic zone causes an increase in export production. The higher DIC concentrations tend to rise pCO_2 and to

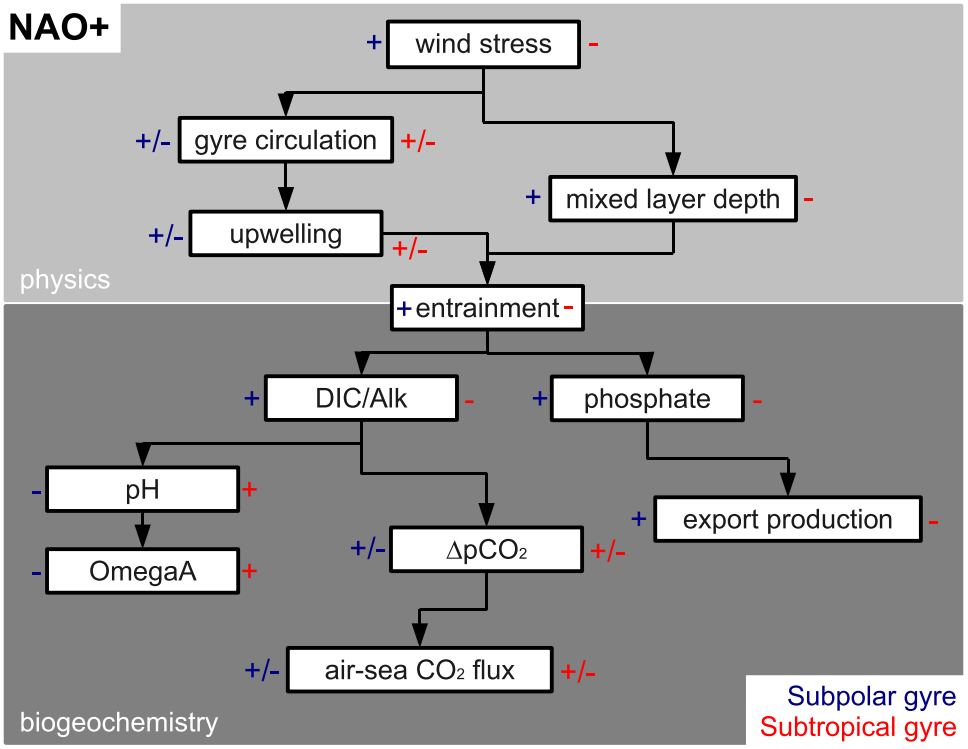

Fig. 10. Response of ocean physics and biogeochemistry in the North Atlantic to NAO^+ forcing. To maintain a certain clarity, the scheme is simplified. For instance, pCO_2 depends not only on DIC and Alk, but also on SST and salinity.

decrease the net air–sea CO_2 flux, as well as pH and OmegaA. However, the links between DIC and surface water pCO_2 and the net air–sea CO_2 flux are not always coherent as changes in surface ocean pCO_2 reflect the balance of partly opposing processes. In contrast to higher DIC, higher Alk and lower temperatures tend to decrease pCO_2 and, consequently, to increase the air–sea flux. In addition, the air–sea gas transfer velocity increases with higher wind speeds. In the western part of the subtropical gyre, characterised by a positive anomaly in SST and a decrease in wind stress and MLD, the reduced entrainment due to stratification results in negative anomalies of DIC and pCO_2 which, in turn, increases the air–sea CO_2 flux. The sign of response to NAO^- is generally the opposite to the response to NAO^+. However, the responses of all six models to NAO^+ versus NAO^- forcing are not strictly symmetric, implying non-linearity in the connection between NAO and the ocean carbon cycle. Typical NAO-driven variations are ± 10 mmol/m^3 in the surface concentration of DIC and alkalinity and ± 8 ppm in the air–sea partial pressure difference. Yet, despite the substantial impact of the NAO on the North Atlantic carbon cycle, the effect on the basin-wide CO_2 flux is small. The integration of the air–sea CO_2 flux over the North Atlantic and the entire winter season results in NAO-related anomalies of up to ± 0.007 PgC, which account for a maximum 5% of the winter mean state. This small total effect is the consequence of compensating fluxes on sub-basin scales (e.g. McKinley et al., 2004; Raynaud et al., 2006). Based on a multichannel singular spectrum analysis (MSSA) of hindcast simulations, Raynaud et al. (2006) show that the subpolar gyre, the intergyre region (the transition area between the subpolar and subtropical gyres) and the subtropical gyre contribute with multipolar anomalies at multiple frequencies that tend to cancel one another in terms of the basin-wide air–sea CO_2 flux. Earlier suggestions of a large NAO-related variability in basin-integrated air–sea flux (Gruber et al., 2002), based on the interpolation of observations from a single location, appear unjustified. These findings highlight the difficulties linked to the regional or even basin-wide extrapolation of local measurements and points out the need for further observation efforts.

Generally speaking, the results of this study are in accordance with observations. The relevance of thermodynamics and vertical convection, especially strong winter mixing, and the associated entrainment of nutrients for the ocean carbon cycle is well established (e.g. Lüger et al., 2004; Tanhua et al., 2006; Olsen et al., 2008; Hartman et al., 2010). Consequently, numerous studies (e.g. Bates

et al., 2002; Gruber et al., 2002; Gonzalez-Davila et al., 2007; Corbière et al., 2007; Schuster and Watson, 2007; Perez et al., 2008; Bates, 2012) provide evidence for a connection between NAO and ocean biogeochemistry in the North Atlantic. For the last decade, a decrease of the North Atlantic carbon sink has been reported (e.g. Lefèvre et al., 2004; Lüger et al., 2006; Bates, 2007; Corbière et al., 2007; Schuster et al., 2009; Takahashi et al., 2009; Metzl et al., 2010). While sea-surface pCO_2 in the subtropics closely followed its raising atmospheric counterpart, in the north, the increase in sea-surface pCO_2 outpaced the atmospheric trend. This resulted in a reduction of ΔpCO_2 and, consequently, the net air–sea flux of CO_2. Schuster and Watson (2007) estimated a large-scale decline of the carbon sink up to $>50\%$ from the mid-1990s to the period 2002–2005, in particular pronounced in the north-east. According to Schuster et al. (2009), the net air–sea CO_2 flux decreased in the area north of approximately 45°N while, in the south, the change was small or even zero. In contrast to the more northern areas, ΔpCO_2 measured at two locations in the subtropical gyre, ESTOC (e.g. Santana-Casiano et al., 2007; Gonzalez-Davila et al., 2010) and BATS (e.g. Bates, 2001, 2007), has remained more or less constant over time. The initial impulse launching research on the connection between NAO and the ocean carbon cycle was the finding that, during this specific period, the NAO was mainly in its negative phase (Corbière et al., 2007; Schuster and Watson, 2007).

The origin of the observed decline in the subpolar carbon sink is still not entirely clear. Proposed explanations include a decrease of biological productivity (Lefèvre et al., 2004), rising SSTs (Corbière et al., 2007), a slowdown of the North Atlantic Current (Thomas et al., 2008), the interplay of the changing buffer capacity of the ocean water and NAO-driven variations in SST, vertical mixing and sea-surface circulation (Schuster and Watson, 2007; Schuster et al., 2009) and changes in surface DIC concentrations due to convective processes (Metzl et al., 2010). Around 20% of the change in pCO_2 observed from the mid-1990s to the early 2000s in the eastern parts of the temperate and subpolar Northern Atlantic are attributable to the observed variability in SST (Schuster and Watson, 2007). In this context, it is interesting to qualitatively compare the subpolar North Atlantic in the NAO^- composites of the six models with the anomalies observed during the period from 1990 to 2006. However, we need to recall that the NAO explains only part of the variability; observed anomalies result from a combination of internal modes, noise, and external forcings. Nevertheless, with regard to ocean physics (i.e. MLD and SST), our NAO^- composites and observations are in qualitative agreement displaying warm anomalies and shallow MLD in the subpolar North Atlantic. Similarly, low DIC and nutrient concentrations are found in the model composites and the observations, apparently the result of decreased entrainment from below. The observed decrease in export production during this NAO^- period is also to some extent mirrored in the model composites. Concerning the air–sea flux of CO_2, the picture is not that uniform. Four of the models (CCSM3, GFDL, BCCR, IPSL) indicate a strengthening of the carbon sink in the respective area while two (CSM1.4, MPIM), qualitatively consistent with observations, indeed show a weakening.

A number of modelling studies have addressed the connection between NAO and North Atlantic Ocean carbon cycle. Most studies utilised global ocean general circulation models (McKinley et al., 2004; Thomas et al., 2008; Ullman et al., 2009; Levine et al., 2011) or coupled ecosystem-circulation models of the North Atlantic (Friedrich et al., 2006; Löptien and Eden, 2010). Concerning the isolation of an NAO-only signal, such ocean-only simulations have a handicap. Since they are forced with observed surface conditions, the forcing imposed on the ocean model includes variability in addition to NAO, e.g. the Tropical Atlantic variability (TAV) or the East Atlantic pattern (EA; Barnston and Livezey, 1987). Moreover, the NAO mode does not evolve freely and in a self-consistent way as in coupled ocean-atmosphere models, hindering the establishment of a clear quantification between NAO forcing and biogeochemical response. On the other hand, the simulated biogeochemical response should closely reflect the observed tracer and air–sea flux evolution in simulations driven by reconstructed surface forcings. These ocean-only model studies are broadly in accordance with the results presented here, although differences remain. The authors identified variations in wind-induced mixing and SST as the main drivers of the response of ocean biogeochemistry. In the subpolar gyre, mixing-driven entrainment of DIC from nutrient-enriched deeper layers to the surface ocean outweighs air–sea gas exchange. In the subtropics, changes in SST and the associated stratification are the dominating factor. Matter of debate are the importance of the biological pump (e.g. McKinley et al., 2004; Löptien and Eden, 2010) and advective transport processes (e.g. Thomas et al., 2008; Raynaud et al., 2006), the latter especially during periods of persistent negative or positive NAO forcing. Raynaud et al. (2006) find the largest correlation between NAO and air–sea CO_2 flux in the subtropical and subpolar gyres near lag zero (r: -0.56 and -0.31, respectively) while, in between, r increases from 0.25 at lag zero to 0.43 at lag 2.5 yr, suggesting that NAO-related advective transport may play a role for the air–sea flux in the intergyre region.

Special attention has been given to the observed decline of the North Atlantic carbon sink. Based on historical simulations with the coupled ocean carbon cycle module of

the CCSM3, Thomas et al. (2008) propose a NAO-induced weakening of the North Atlantic Current and the associated decrease in transport of warm, saline subtropical waters to the north-east as the main cause. In accordance with our results, Ullman et al. (2009) utilised the MIT Ocean General Circulation Model to identify changes in SST (subtropics) and dynamical processes, primarily entrainment of DIC (subpolar gyre), as the main drivers of ocean pCO_2. However, they were not able to explain the observations. Instead, their model indicated an increase in carbon uptake in the North Atlantic – as do four out of six of our models during NAO^-. Further evidence for the importance of vertical mixing is provided by recent studies by Levine et al. (2011) and Patara et al. (2011). Regarding the link between NAO and advective transport, it is interesting to note that the observed NAO index varies significantly with season and, e.g. during winter 2007/2008 (2008/2009), switched from positive (negative) DJF values to a negative (positive) MAM state.

Only recently, the biogeochemical response to NAO has been isolated using a single AOGCM (Patara et al., 2011). These authors argue that the drivers behind the response of biogeochemistry differ, depending on the timescale considered. They state that, while interannual variations are dominated by vertical mixing, ocean circulation gains impact on decadal time scales.

5. Conclusion

The response of the ocean carbon cycle to the NAO has been analysed based on control runs of six Earth System Models. The results are consistent, though relative and absolute magnitudes differ among models and regions. The response of ocean biogeochemistry in the North Atlantic is a seesaw pattern between the subtropical and subpolar gyre. This pattern emerges instantaneously (<3 months) and is mainly driven by vertical exchange between the surface and the thermocline. The overall effect on the basin-wide CO_2 flux is small. Reasons are compensating fluxes on the sub-basin scale. All models show non-linear behaviour in response to positive and negative states of the NAO.

Our study shows that the NAO has significant impact on the ocean carbon cycle in the North Atlantic, which is in accordance with a recent observation-based study (McKinley et al., 2011) quantifying the time period necessary for a long-term trend to overcome decadal-scale variability with 25 yr. Since observations are scarce and limited in time, this highlights (1) the importance of a sound consideration of the NAO in the interpretation of observations and (2) the necessity of model studies to thoroughly investigate such connections between climate and ocean carbon cycle. An issue of interest is the hypothesised future shift of the NAO to a more positive phase (e.g. Hegerl et al., 2007; Bader et al., 2011), which might have a substantial impact on the future evolution of the North Atlantic carbon sink.

6. Acknowledgments

We thank Andreas Born, Marco Steinacher, Aida F. Ríos, Fiz F. Pérez and Jón Ólafsson for discussion and constructive comments. The research leading to these results was supported through EU FP7 project CARBOCHANGE 'Changes in carbon uptake and emissions by oceans in a changing climate' which received funding from the European Community's Seventh Framework Programme under grant agreement no. 264879. Additional support was received from the Swiss National Science Foundation. TLF was supported by BP through the Carbon Mitigation Initiative at Princeton University. N. Metzl also acknowledges support from the French national programme LEFE/INSU. This is publication nr. A406 from the Bjerknes Centre for Climate Research (BCCR), and it is a contribution to the Centre for Climate Dynamics (SKD) at BCCR. Simulations with CSM1.4 and CCSM3 were carried out at the Swiss National Supercomputing Centre in Manno, Switzerland.

References

Anderson, J., Balaji, V., Broccoli, A., Cooke, W., Delworth, T. and co-authors. 2004. The new GFDL global atmosphere and land model AM2-LM2: evaluation with prescribed SST simulations. *J. Clim.* **17**, 4641–4673.

Assmann, K. M., Bentsen, M., Segschneider, J. and Heinze, C. 2010. An isopycnic ocean carbon cycle model. *Geosci. Model Dev.* **3**, 143–167.

Aumont, O., Maier-Reimer, E., Blain, S. and Monfray, P. 2003. An ecosystem model of the global ocean including Fe, Si, P colimitations. *Global Biogeochem. Cy.* **17**, 1–23.

Bader, J., Mesquita, M. D. S., Hodges, K. I., Keenlyside, N., Østerhus, S. and co-authors. 2011. A review on Northern Hemisphere sea-ice, storminess and the North Atlantic Oscillation: observations and projected changes. *Atmos. Res.* **101**, 809–834.

Baldwin, M. P., Stephenson, D. B. and Jolliffe, I. T. 2009. Spatial weighting and iterative projection methods for EOFs. *J. Clim* **22**, 234–243.

Barnston, A. and Livezey, R. 1987. Classification, Seasonality and Persistence of Low-Frequency Atmospheric Circulation Patterns. *Mon. Weather Rev.* **115**, 1083–1126.

Bates, N. 2001. Interannual variability of oceanic CO_2 and biogeochemical properties in the Western North Atlantic subtropical gyre. *Deep Sea Res. Part II* **48**, 1507–1528.

Bates, N., Pequignet, A., Johnson, R. and Gruber, N. 2002. A short-term sink for atmospheric CO_2 in subtropical mode water of the North Atlantic Ocean. *Nature* **420**, 489–493.

Bates, N. R. 2007. Interannual variability of the oceanic CO_2 sink in the subtropical gyre of the North Atlantic Ocean over the last 2 decades. *J. Geophys. Res. Oceans* **112**, 1–26.

Bates, N. R. 2012. Multi-decadal uptake of carbon dioxide into subtropical mode water of the North Atlantic Ocean. *Biogeosciences* **9**, 2649–2659.

Bjerknes, J. 1964. Atlantic air-sea interaction. *Adv. Geophys* **10**, 1–82.

Blackford, J. C. and Gilbert, F. J. 2007. pH variability and CO_2 induced acidification in the North Sea. *J. Marine. Syst.* **64**, 229–241.

Blackmon, M., Boville, B., Bryan, F., Dickinson, R., Gent, P. and co-authors. 2001. The Community Climate System Model. *B. Am. Meteorol. Soc.* **82**, 2357–2376.

Bleck, R., Rooth, C., Hu, D. and Smith, L. 1992. Salinity-driven thermocline transients in a wind- and thermohaline-forced Isopycnic Coordinate Model of the North Atlantic. *J. Phys. Oceanogr.* **22**, 1486–1505.

Boden, T., Marland, G. and Andres, R. 2010. *Global, Regional, and National Fossil-Fuel CO_2 Emissions*. Carbon Dioxide Information Analysis Center, Oak Ridge, Tenn., USA.

Boville, B., Kiehl, J., Rasch, P. and Bryan, F. 2001. Improvements to the NCAR CSM-1 for transient climate simulations. *J. Clim.* **14**, 164–179.

Briegleb, B. P., Bitz, C. M., Hunke, E. C., Lipscomb, W. H., Holland, M. M. and co-authors. 2004. *Scientific Description of the Sea Ice Component in the Community Climate System Model Version Three*. Technical Report NCAR/TN-463+STR, National Center for Atmospheric Research, Boulder, USA.

Cayan, D. R. 1992. Latent and sensible heat flux anomalies over the northern oceans: driving the sea surface temperature. *J. Phys. Oceanogr.* **22**, 859–881.

Collins, W. D., Bitz, C. M., Blackmon, M. L., Bonan, G. B., Bretherton, C. S. and co-authors. 2006a. The community climate system model version 3 (CCSM3). *J. Clim.* **19**, 2122–2143.

Collins, W., Rasch, P., Boville, B., Hack, J., McCaa, J. and co-authors. 2006b. The formulation and atmospheric simulation of the community atmosphere model version 3 (CAM3). *J. Clim.* **19**, 2144–2161.

Compo, G. P., Whitaker, J. S., Sardeshmukh, P. D., Matsui, N., Allan, R. J. and co-authors. 2011. The Twentieth century reanalysis project. *Q. J. Roy. Meteor. Soc.* **137**, 1–28.

Corbière, A., Metzl, N., Reverdin, G., Brunet, C. and Takahashi, T. 2007. Interannual and decadal variability of the oceanic carbon sink in the North Atlantic subpolar gyre. *Tellus B* **59**, 168–178.

Crutzen, P. J. and Stoermer, E. F. 2000. The 'anthropocene'. *IGBP Newsletter* **41**, 17–18.

Cullen, H., D'Arrigo, R. D., Cook, E. R. and Mann, M. E. 2001. Multiproxy reconstructions of the North Atlantic Oscillation. *Paleoceanography* **16**, 27–39.

Curry, R. and McCartney, M. 2001. Ocean gyre circulation changes associated with the North Atlantic Oscillation. *J. Phys. Oceanogr.* **31**, 3374–3400.

Delworth, T., Broccoli, A., Rosati, A., Stouffer, R., Balaji, V. and co-authors. 2006. GFDL's CM2 global coupled climate models. Part I: formulation and simulation characteristics. *J. Clim.* **19**, 643–674.

Dickson, R., Lazier, J., Meincke, J., Rhines, P. and Swift, J. 1996. Long-term coordinated changes in the convective activity of the North Atlantic. *Prog. Oceanogr.* **38**, 241–295.

Dolman, A. J., Van der Werf, G. R., Van der Molen, M. K., Ganssen, G., Erisman, J. W. and co-authors. 2010. A carbon cycle science update since IPCC AR-4. *Ambio* **39**, 402–412.

Doney, S. C., Lindsay, K., Fung, I. and John, J. 2006. Natural variability in a stable, 1000-yr global coupled climate-carbon cycle simulation. *J. Clim.* **19**, 3033–3054.

Dunne, J., Armstrong, R., Gnanadesikan, A. and Sarmiento, J. 2005. Empirical and mechanistic models for the particle export ratio. *Global Biogeochem. Cy.* **19**, 1–16.

Dunne, J. P., Sarmiento, J. L. and Gnanadesikan, A. 2007. A synthesis of global particle export from the surface ocean and cycling through the ocean interior and on the seafloor. *Global Biogeochem. Cy.* **21**, 1–16.

Eppley, R. W. 1972. Temperature and phytoplankton growth in the sea. *Fish B-NOAA* **70**, 1063–1085.

Fasham, M., Balino, B., Bowles, M., Anderson, R., Archer, D. and co-authors. 2001. A new vision of ocean biogeochemistry after a decade of the joint global ocean flux study (JGOFS). *Ambio* **10**, 4–31.

Flatau, M., Talley, L. and Niiler, P. 2003. The North Atlantic Oscillation, surface current velocities, and SST changes in the subpolar North Atlantic. *J. Climate* **16**, 2355–2369.

Friedrich, T., Oschlies, A. and Eden, C. 2006. Role of wind stress and heat fluxes in interannual-to-decadal variability of air-sea CO_2 and O_2 fluxes in the North Atlantic. Geophys. Res. Lett. **33**, 1–5.

Friis, K., Körtzinger, A. and Wallace, D. 2003. The salinity normalization of marine inorganic carbon chemistry data. *Geophys. Res. Lett.* **30**, 1–4.

Frölicher, T. L. and Joos, F. 2010. Reversible and irreversible impacts of greenhouse gas emissions in multi-century projections with the NCAR global coupled carbon cycle-climate model. *Clim. Dyn.* **35**, 1439–1459.

Frölicher, T. L., Joos, F., Plattner, G. K., Steinacher, M. and Doney, S. C. 2009. Natural variability and anthropogenic trends in oceanic oxygen in a coupled carbon cycle-climate model ensemble. *Global Biogeochem. Cy.* **23**, 1–15.

Fung, I., Doney, S., Lindsay, K. and John, J. 2005. Evolution of carbon sinks in a changing climate. *PNAS* **102**, 11201–11206.

Furevik, T., Bentsen, M., Drange, H., Kindem, I., Kvamstø, N. and co-authors. 2003. Description and evaluation of the Bergen climate model: ARPEGE coupled with MICOM. *Clim. Dyn.* **21**, 27–51.

Garcia, H. E., Locarnini, R. A., Boyer, T. P., Antonov, J. I., Zweng, M. M. and co-authors. 2010. World Ocean Atlas 2009, Volume 4: nutrients (phosphate, nitrate, silicate). In: *NOAA Atlas NESDIS 71* (ed. Levitus, S.) US Government Printing Office, Washington, DC.

Gent, P., Bryan, F., Danabasoglu, G., Doney, S., Holland, W. and co-authors. 1998. The NCAR Climate System Model global ocean component. *J. Clim.* **11**, 1287–1306.

Gerber, M. and Joos, F. 2010. Carbon sources and sinks from an ensemble Kalman filter ocean data assimilation. *Global Biogeochem. Cycles* **24**, 1–14.

Gonzalez-Davila, M., Santana-Casiano, J. M. and Gonzalez-Davila, E. F. 2007. Interannual variability of the upper ocean carbon cycle in the northeast Atlantic ocean. *Geophys. Res. Lett.* **34**, 1–7.

Gonzalez-Davila, M., Santana-Casiano, J. M., Rueda, M. J. and Llinas, O. 2010. The water column distribution of carbonate system variables at the ESTOC site from 1995 to 2004. *Biogeosciences* **7**, 3067–3081.

Griffies, S. M., Harrison, M. J., Pacanowski, R. C. and Rosati, A. 2004. *A Technical Guide to MOM4*. GFDL Ocean Group Technical Report, Geophysical Fluid Dynamics Laboratory, Princeton, USA.

Gruber, N., Keeling, C. and Bates, N. 2002. Interannual variability in the North Atlantic ocean carbon sink. *Science* **298**, 2374–2378.

Gruber, N. and Sarmiento, J. L. 2002. Large-scale biogeochemical-physical interactions in elemental cycles. In: *The Sea: Biological-Physical Interactions in the Oceans* (eds. J. J. M. A. R. Robinson and B. J. Rothschild) Vol. 12, John Wiley & Sons, 337–399.

Hartman, S. E., Larkin, K. E., Lampitt, R. S., Lankhorst, M. and Hydes, D. J. 2010. Seasonal and inter-annual biogeochemical variations in the Porcupine Abyssal Plain 2003–2005 associated with winter mixing and surface circulation. *Deep Sea Res. Part II* **57**, 1303–1312.

Hegerl, G. C., Zwiers, F. W., Braconnot, P., Gillett, N., Luo, Y. and co-authors. 2007. Understanding and Attributing Climate Change. In: *Climate Change 2007: The Physical Science Basis. Contribution of Working Group I to the 4th Assessment Report of the Intergovernmental Panel on Climate Change* (eds. Solomon, S., D. Qin, M. Manning, Z. Chen, M. Marquis, K.B. Averyt, M. Tignor and H.L. Miller, Cambridge University Press, Cambridge, United Kingdom and New York, NY, USA, 663–746.

Henson, S. A., Sarmiento, J. L., Dunne, J. P., Bopp, L., Lima, I. and co-authors. 2010. Detection of anthropogenic climate change in satellite records of ocean chlorophyll and productivity. *Biogeosciences* **7**, 621–640.

Hourdin, F., Musat, I., Bony, S., Braconnot, P., Codron, F. and co-authors. 2006. The LMDZ4 general circulation model: climate performance and sensitivity to parametrized physics with emphasis on tropical convection. *Clim. Dyn.* **27**, 787–813.

Hurrell, J. W. and Deser, C. 2009. North Atlantic climate variability: the role of the North Atlantic Oscillation. *J. Marine Syst.* **78**, 28–41.

Jakobsen, P., Ribergaard, M., Quadfasel, D., Schmith, T. and Hughes, C. 2003. Near-surface circulation in the northern North Atlantic as inferred from Lagrangian drifters: variability from the mesoscale to interannual. *J. Geophys. Res. Oceans* **108**.

Joos, F. and Spahni, R. 2008. Rates of change in natural and anthropogenic radiative forcing over the past 20,000 years. *PNAS* **105**, 1425–1430.

Key, R., Kozyr, A., Sabine, C., Lee, K., Wanninkhof, R. and co-authors. 2004. A global ocean carbon climatology: results from Global Data Analysis Project (GLODAP). *Global Biogeochem. Cy.* **18**, 1–23.

Key, R. M., Tanhua, T., Olsen, A., Hoppema, M., Jutterström, S. and co-authors. 2010. The CARINA data synthesis project: introduction and overview. *Earth Syst. Sci. Data.* **2**, 105–121.

Kiehl, J., Hack, J., Bonan, G., Boville, B., Williamson, D. and co-authors. 1998. The National Center for Atmospheric Research Community Climate Model: CCM3. *J. Clim.* **11**, 1131–1149.

Krinner, G., Viovy, N., de Noblet-Ducoudre, N., Ogee, J., Polcher, J. and co-authors. 2005. A dynamic global vegetation model for studies of the coupled atmosphere-biosphere system. *Global Biogeochem. Cy.* **19**, 1–33.

Latif, M., Kleeman, R. and Eckert, C. 1997. Greenhouse warming, decadal variability, or El Niño? An attempt to understand the anomalous 1990s. *J. Clim* **10**, 2221–2239.

Lefèvre, N., Watson, A., Olsen, A., Rios, A., Perez, F. and co-authors. 2004. A decrease in the sink for atmospheric CO_2 in the North Atlantic. *Geophys. Res. Lett.* **31**.

Levine, N. M., Doney, S. C., Lima, I., Wanninkhof, R., Bates, N. R. and co-authors. 2011. The impact of the North Atlantic Oscillation on the uptake and accumulation of anthropogenic CO_2 by North Atlantic Ocean mode waters. *Global Biogeochem. Cy.* **25**, 1–15.

Löptien, U. and Eden, C. 2010. Multidecadal CO_2 uptake variability of the North Atlantic. *J. Geophys. Res. Atmos.* **115**, 1–16.

Lueker, T., Dickson, A. and Keeling, C. 2000. Ocean pCO_2 calculated from dissolved inorganic carbon, alkalinity, and equations for K-1 and K-2: validation based on laboratory measurements of CO_2 in gas and seawater at equilibrium. *Mar. Chem.* **70**, 105–119.

Lüger, H., Wallace, D., Körtzinger, A. and Nojiri, Y. 2004. The pCO_2 variability in the midlatitude North Atlantic ocean during a full annual cycle. *Global Biogeochem. Cy.* **18**, 1–16.

Lüger, H., Wanninkhof, R., Wallace, D. and Körtzinger, A. 2006. CO_2 fluxes in the subtropical and subarctic North Atlantic based on measurements from a volunteer observing ship. *J. Geophys. Res. Oceans* **111**, 1–10.

Lüthi, D., Le Floch, M., Bereiter, B., Blunier, T., Barnola, J.-M. and co-authors. 2008. High-resolution carbon dioxide concentration record 650,000–800,000 years before present. *Nature* **453**, 379–382.

Madec, G., Delecluse, P., Imbard, M. and Lévy, M. 1998. OPA 8.1 Ocean General Circulation Model reference manual. Note du Pole de modélisation, No. 11, Institut Pierre-Simon Laplace (IPSL), Paris, France.

Maier-Reimer, E., Kriest, I., Segschneider, J. and Wetzel, P. 2005. *The HAMburg Ocean Carbon Cycle model HAMOCC5.1*. Technical description. Max-Planck-Institut für Meteorologie, Hamburg, Germany.

Marshall, J., Johnson, H. and Goodman, J. 2001. A study of the interaction of the North Atlantic Oscillation with ocean circulation. *J. Clim* **14**, 1399–1421.

Marsland, S., Haak, H., Jungclaus, J., Latif, M. and Roske, F. 2003. The Max-Planck-Institute global ocean/sea ice model with orthogonal curvilinear coordinates. *Ocean Model.* **5**, 91–127.

McKinley, G. A., Fay, A. R., Takahashi, T. and Metzl, N. 2011. Convergence of atmospheric and North Atlantic carbon dioxide trends on multidecadal timescales. *Nat. Geosci.* **4**, 606–610.

McKinley, G. A., Follows, M. J. and Marshall, J. 2004. Mechanisms of air-sea CO_2 flux variability in the equatorial Pacific and the North Atlantic. *Global Biogeochem. Cy.* **18**, 1–14.

Metzl, N., Corbiere, A., Reverdin, G., Lenton, A., Takahashi, T. and co-authors. 2010. Recent acceleration of the sea surface fCO_2 growth rate in the North Atlantic subpolar gyre (1993–2008) revealed by winter observations. *Global Biogeochem. Cy.* **24**, 1–13.

Moore, J., Doney, S.and Lindsay, K. 2004. Upper ocean ecosystem dynamics and iron cycling in a global three-dimensional model. *Global Biogeochem. Cy.* **18**, 1–21.

Najjar, R. G., Jin, X., Louanchi, F., Aumont, O., Caldeira, K. and co-authors. 2007. Impact of circulation on export production, dissolved organic matter, and dissolved oxygen in the ocean: results from phase II of the ocean carbon-cycle model intercomparison project (OCMIP-2). *Global Biogeochem. Cy.* **21**, 1–22.

Olafsson, J. 2007a. *Iceland Sea Cruise Data from the 1991–2006 Cruises, CARINA Data Set*. Carbon Dioxide Information Analysis Center, Oak Ridge, Tennessee. Online at http://cdiac.ornl.gov/ftp/oceans/CARINA/IcelandSea/

Olafsson, J. 2007b. *Irminger Sea Cruise Data from the 1991–2006 Cruises, CARINA Data Set*. Carbon Dioxide Information Analysis Center, Oak Ridge, Tenn., USA. Online at http://cdiac.ornl.gov/ftp/oceans/CARINA/IrmingerSea/

Oleson, K., Dai, Y., Bonan, G., Bosilovich, M., Dickinson, R. and co-authors. 2004. *Technical description of the Community Land Model (CLM)*. NCAR Tech. Note NCAR/TN-461+STR, National Center for Atmospheric Research (NCAR), Boulder, USA.

Olsen, A., Brown, K. R., Chierici, M., Johannessen, T. and Neill, C. 2008. Sea-surface CO_2 fugacity in the subpolar North Atlantic. *Biogeosciences* **5**, 535–547.

Osborn, T. 2004. Simulating the winter North Atlantic Oscillation: the roles of internal variability and greenhouse gas forcing. *Clim. Dyn.* **22**, 605–623.

Parker, D., Folland, C., Scaife, A., Knight, J., Colman, A. and co-authors. 2007. Decadal to multidecadal variability and the climate change background. *J. Geophys. Res. Atmos* **112**, 1–18.

Patara, L., Visbeck, M., Masina, S., Krahmann, G. and Vichi, M. 2011. Marine biogeochemical responses to the North Atlantic Oscillation in a coupled climate model. *J. Geophys. Res. Oceans* **116**, 1–20.

Perez, F. F., Vazquez-Rodriguez, M., Louarn, E., Padin, X. A., Mercier, H. and co-authors. 2008. Temporal variability of the anthropogenic CO_2 storage in the Irminger Sea. *Biogeosciences* **5**, 1669–1679.

Pinto, J. G. and Raible, C. C. 2012. Past and recent changes in the North Atlantic Oscillation. *Wiley Interdiscip. Rev. Clim. Change* **3**, 79–90.

Plattner, G., Joos, F., Stocker, T. and Marchal, O. 2001. Feedback mechanisms and sensitivities of ocean carbon uptake under global warming. *Tellus B* **53**, 564–592.

Raible, C., Luksch, U., Fraedrich, K. and Voss, R. 2001. North Atlantic decadal regimes in a coupled GCM simulation. *Clim. Dyn.* **18**, 321–330.

Randerson, J., Thompson, M., Conway, T., Fung, I. and Field, C. 1997. The contribution of terrestrial sources and sinks to trends in the seasonal cycle of atmospheric carbon dioxide. *Global Biogeochem. Cy.* **11**, 535–560.

Raynaud, S., Orr, J. C., Aumont, O., Rodgers, K. B. and Yiou, P. 2006. Interannual-to-decadal variability of North Atlantic air-sea CO_2 fluxes. *Ocean Sci.* **2**, 43–60.

Redfield, A. C., Ketchum, B. H. and Richards, F. A. 1963. The influence of organisms on the composition of seawater. *Interscience* **2**, 26–77.

Robbins, P. 2001. Oceanic carbon transport carried by freshwater divergence: are salinity normalizations useful? *J. Geophys. Res. Oceans* **106**, 30939–30946.

Roy, T., Bopp, L., Gehlen, M., Schneider, B., Cadule, P. and co-authors. 2011. Regional impacts of climate change and atmospheric CO_2 on future ocean carbon uptake: a multi-model linear feedback analysis. *J. Climate* **24**, 2300–2318.

Sabine, C. L., Feely, R. A., Gruber, N., Key, R. M., Lee, K. and co-authors. 2004. The Oceanic Sink for Anthropogenic CO_2. *Science* **305**, 367–371.

Santana-Casiano, J. M., Gonzalez-Davila, M., Rueda, M.-J., Llinas, O. and Gonzalez-Davila, E.-F. 2007. The interannual variability of oceanic CO_2 parameters in the northeast Atlantic subtropical gyre at the ESTOC site. *Global Biogeochem. Cy.* **21**, 1–16.

Sarmiento, J. L., Gloor, M., Gruber, N., Beaulieu, C., Jacobson, A. R. and co-authors. 2010. Trends and regional distributions of land and ocean carbon sinks. *Biogeosciences* **7**, 2351–2367.

Schneider, B., Bopp, L., Gehlen, M., Segschneider, J., Frölicher, T. L. and co-authors. 2008. Climate-induced interannual variability of marine primary and export production in three global coupled climate carbon cycle models. *Biogeosciences* **5**, 597–614.

Schuster, U. and Watson, A. J. 2007. A variable and decreasing sink for atmospheric CO_2 in the North Atlantic. *J. Geophys. Res. Oceans* **112**, 1–10.

Schuster, U., Watson, A. J., Bates, N. R., Corbière, A., Gonzalez-Davila, M. and co-authors. 2009. Trends in North Atlantic sea-surface fCO_2 from 1990 to 2006. *Deep Sea Res. Part II* **56**, 620–629.

Sitch, S., Smith, B., Prentice, I., Arneth, A., Bondeau, A. and co-authors. 2003. Evaluation of ecosystem dynamics, plant geography and terrestrial carbon cycling in the LPJ dynamic global vegetation model. *Global Change Biol.* **9**, 161–185.

Smith, R. and Gent, P. 2004. *The Parallel Ocean Program (POP) Reference Manual*. Technical Report, LAUR-02-2484, Los Alamos National Laboratory (LANL), USA.

Steinacher, M., Joos, F., Frölicher, T. L., Bopp, L., Cadule, P. and co-authors. 2010. Projected 21st century decrease in marine productivity: a multi-model analysis. *Biogeosciences* **7**, 979–1005.

Takahashi, T., Sutherland, S. C., Wanninkhof, R., Sweeney, C., Feely, R. A. and co-authors. 2009. Climatological mean and decadal change in surface ocean pCO_2, and net sea-air CO_2 flux over the global oceans. *Deep Sea Res. Part II* **56**, 554–577.

Tanhua, T., Biastoch, A., Körtzinger, A., Lüger, H., Böning, C. and co-authors. 2006. Changes of anthropogenic CO_2 and CFCs in the North Atlantic between 1981 and 2004. *Global Biogeochem. Cy.* **20**, 1–13.

Terray, L., Thual, O., Belamari, S., Déqué, M., Dandin, P. and co-authors. 1995. Climatology and interannual variability simulated by the ARPEGE-OPA model. *Clim. Dyn.* **11**, 487–505.

Thomas, H., Prowe, A. E. F., Lima, I. D., Doney, S. C., Wanninkhof, R. and co-authors. 2008. Changes in the North Atlantic Oscillation influence CO_2 uptake in the North Atlantic over the past 2 decades. *Global Biogeochem. Cy.* **22**, 1–13.

Tjiputra, J. F., Assmann, K., Bentsen, M., Bethke, I., Otterå, O. H. and co-authors. 2010. Bergen Earth system model (BCM-C): model description and regional climate-carbon cycle feedbacks assessment. *Geosci. Model Dev.* **3**, 123–141.

Tjiputra, J. F., Olsen, A., Assmann, K., Pfeil, B. and Heinze, C. 2012. A model study of the seasonal and long-term North Atlantic surface pCO_2 variability. *Biogeosciences* **9**, 907–923.

Ullman, D. J., McKinley, G. A., Bennington, V. and Dutkiewicz, S. 2009. Trends in the North Atlantic carbon sink: 1992–2006. *Global Biogeochem. Cy.* **23**, 1–16.

Visbeck, M., Chassignet, E., Curry, R., Delworth, T., Dickson, R. and co-authors. 2003. The ocean's response to North Atlantic Oscillation variability. In: *The North Atlantic Oscillation, Climatic Significance and Environmental Impact* (eds. J. Hurrell, Y. Kushnir, G. Ottersen and M. Visbeck) Vol. 134 of Geophysical Monograph, American Geophysical Union, Washington, DC, pp. 113–146.

Wanner, H., Brönnimann, S., Casty, C., Gyalistras, D., Luterbacher, J. and co-authors. 2001. North Atlantic Oscillation – concepts and studies. *Surv. Geophys.* **22**, 321–382.

Wanninkhof, R. 1992. Relationship between wind speed and gas exchange over the ocean. *J. Geophys. Res. Oceans* **97**, 7373–7382.